Cytotoxic CD4$^+$ T cells driven by T-cell intrinsic IL-18R/MyD88 signaling predominantly infiltrate *Trypanosoma cruzi*-infected hearts

Carlos-Henrique. D. Barbosa[1,2], Ariel Gomes[1,3]*, Fábio B. Canto[1,4]*, Layza M. Brandão[1], Jéssica R. Lima[1], Guilherme A. Melo[1], Alessandra Granato[1,5], Eula G.A. Neves[6], Walderez O. Dutra[6], Ana C. Oliveira[7], Alberto Nóbrega[1] and Maria Bellio[1]**.

[1]Department of Immunology, Instituto de Microbiologia Paulo de Góes, Universidade Federal do Rio de Janeiro (UFRJ), Rio de Janeiro, RJ, 21941-902 Brazil; Ph: +55-21-987496559

[2]present address: Department of Microbiology & Immunology, Chicago Medical School, Rosalind Franklin University of Medicine and Science, Chicago, IL, USA.

[3]present address: Faculdade de Medicina da Universidade Estácio de Sá, Angra dos Reis, RJ Brazil.

[4]present address: Departamento de Imunobiologia, Instituto de Biologia, Universidade Federal Fluminense (UFF) Niterói, RJ 24210-350, Brazil.

[5]present address: The Hospital for Sick Children - Genetics and Genome Biology. Toronto, ON, Canada

[6]Laboratório de Biologia das Interações Celulares, ICB, Universidade Federal de Minas Gerais, Belo Horizonte, MG, Brazil

[7]Instituto de Biofísica Carlos Chagas Filho, UFRJ, Rio de Janeiro, RJ, Brazil.

Keywords: Infectious disease**,** cytotoxicity, myocarditis, parasite, tissue immunity.

* These two authors contributed equally to this work

***Corresponding Author and Lead Contact*:

e-mail: belliom@micro.ufrj.br or mariabellioufrj@gmail.com

Abstract:

Increasing attention has been directed to cytotoxic $CD4^+$ T cells (CD4CTLs) in different pathologies, both in humans and mice. The impact of CD4CTLs in immunity and the mechanisms controlling their generation, however, remain poorly understood. Here, for the first time, we showed that CD4CTLs abundantly differentiate during mouse infection with an intracellular parasite. CD4CTLs appear in the spleen in parallel to Th1 cells, display pathogen-derived peptide-specific cytotoxicity against antigen-presenting cells and express immunoregulatory and/or exhaustion markers. We demonstrated that CD4CTL absolute numbers and activity are severely reduced in both *Myd88*$^{-/-}$ and *Il18ra*$^{-/-}$ mice. Of note, the infection of mixed-bone marrow chimeras revealed that WT, but not *Myd88*$^{-/-}$, cells transcribe the CD4CTL gene signature and that *Il18ra*$^{-/-}$$CD4^+$ phenocopy *Myd88*$^{-/-}$$CD4^+$ T cells. Moreover, the adoptive transfer of WT $CD4^+GzB^+$ T cells to susceptible *Il18ra*$^{-/-}$ mice increased their survival. Importantly, cells expressing the CD4CTL phenotype predominate among $CD4^+$ T cells infiltrating the infected cardiac tissue, are increased in the circulation of Chagas patients and their frequency correlates with severe cardiomyopathy. Our findings describe CD4CTLs as a major player in immune response to a relevant human pathogen and disclose T-cell intrinsic IL-18R/MyD88 signaling as a key pathway controlling the magnitude of the CD4CTL response.

51 **Introduction:**

52 CD4CTLs are present in viral infections, cancer and autoimmunity (Cheroutre &
53 Husain, 2013; Juno et al., 2017; Takeuchi & Saito, 2017). Although more frequently
54 found in chronic conditions, CD4CTLs have also been described during acute viral
55 infection (Brien et al., 2008; Brown et al., 2012; Fang et al., 2012; Jellison, et al., 2005;
56 Wilkinson et al., 2012). At present, however, there are few studies on the CD4CTL
57 response to infection with non-viral intracellular pathogens (Burel et al., 2016; Canaday
58 et al., 2001; Kotov et al., 2018; Krueger et al., 2021). The role of CD4CTLs in
59 immunity against intracellular parasites and the mechanisms operating in the generation
60 and maintenance of this cell subset are poorly understood.

61 Following the recognition of the cognate antigen-MHC complex, and under the
62 influence of cytokines secreted by antigen presenting cells (APCs), naïve $CD4^+$ T cells
63 proliferate and differentiate into diverse subsets, such as Tfh, Th1, Th2 or Th17, with
64 varied effector functions. Different pathogen-derived molecular patterns (PAMPs) elicit
65 distinct innate immune pathways, resulting in tailored Th responses against the
66 infectious agent (Kara et al., 2014). Interestingly, increasing heterogeneity in the
67 transcriptional profile of effector $CD4^+$ T cells, dictated in a microbe-specific manner,
68 has been recently found in the gut (Kiner et al., 2021). Additionally, tissue-derived
69 factors can also be involved in defining $CD4^+$ T cell phenotypes (Poholek, 2021). In this
70 context, the mechanism regulating the differentiation of CD4CTLs remains an open and
71 relevant question. Although some authors consider CD4CTLs functional variants of
72 Th1 cells, there is also evidence that CD4CTLs might constitute a Th1-independent
73 subset, directly differentiating from naïve $CD4^+$ T cell precursors, or even a
74 heterogeneous population congregating cytolytic cells that originate from different T-

75 cell subsets, such as Treg and Th2 cells [reviewed in (Cheroutre & Husain, 2013) and
76 (Takeuchi & Saito, 2017)].

77 Receptors members of the TLR and IL-1R families are upstream of the MyD88
78 adaptor molecule and are expressed both in myeloid and lymphoid cell lineages.
79 MyD88-dependent signaling in innate cells can influence Th1 cell differentiation, by
80 inducing the release of IL-12 or IFN-γ (Joffre et al., 2009; Takeda et al., 1998), The T-
81 cell intrinsic MyD88 adaptor function was also shown to be essential for the Th1
82 response in different contexts. The identity of the receptor acting upstream MyD88 on T
83 cells, however, was not always determined (Frazer et al., 2013; LaRosa et al., 2008) and
84 remains a matter of debate. Early *in vitro* studies have shown that IL-18 synergizes with
85 IL-12 in the induction of IFN-γ production and T-bet expression by $CD4^+$ T cells and,
86 therefore, impacts on Th1 development (Robinson et al., 1997). Intriguingly, however,
87 the IL-18 contribution for a robust Th1 response *in vivo* has not always been confirmed
88 (Haring & Harty, 2009; Monteforte et al., 2000). ST2 (IL-33 receptor) and IL-1R have
89 also been implicated in the establishment of Th1 responses to viral infection (Baumann
90 et al., 2015) and immunization (Ben-Sasson et al., 2009; Schenten et al., 2014),
91 respectively. Recently, our group has disclosed the crucial role of T cell-intrinsic IL-
92 18R/MyD88 signaling for the reinforcement and maintenance of the Th1 program *in*
93 *vivo,* in response to mouse infection with *Trypanosoma cruzi,* where Th1 cells have a
94 key protective function (Oliveira et al., 2017; Rodrigues et al., 2012).

95 *T. cruzi* is an intracellular protozoan parasite and the etiologic agent of Chagas
96 disease (*American trypanosomiasis*), one of the most important parasitic diseases in the
97 Western Hemisphere. Chagas disease is an important cause of heart failure, stroke,
98 arrhythmia, and sudden death, being the leading cause of cardiomyopathy among
99 younger individuals in Latin America (Bern, 2015; Nunes et al., 2018). Here, we

100 showed that $CD4^+$ T lymphocytes with CD4CTL phenotype are abundantly present in
101 the spleen of mice infected with *T. cruzi*, displaying *in vitro* and *in vivo* Ag-specific
102 cytotoxicity against APCs. Of note, we found that cells with CD4CTL phenotype
103 predominate among $CD4^+$ T lymphocytes infiltrating the infected cardiac tissue. Using
104 mixed bone marrow (mix-BM) chimeras, we showed that T cell-intrinsic IL-
105 18R/MyD88 signaling plays a crucial role on the expansion/survival of $CD4^+$ T cells
106 expressing the CD4CTL gene signature *in vivo*. In accordance with results obtained in
107 mix-BM chimeras, we found that absolute numbers of $CD4^+$ T cells displaying
108 cytotoxic markers and activity were severely reduced in *Myd88*$^{-/-}$ and *Il18ra*$^{-/-}$ mouse
109 lineages. Moreover, the adoptive transfer of WT $CD4^+GzB^+$ T cells to *Il18ra*$^{-/-}$ mice
110 increased the survival of this susceptible mouse strain to infection. Interestingly, the
111 majority of $CD4^+GzB^+$ T cells in WT infected mice express high levels of
112 immunoregulatory molecules such as Tim-3, Lag-3 and CD39. Finally, and importantly,
113 we detected the presence of $CD4^+$ T cells expressing perforin in the circulation of
114 patients with the severe cardiac form of Chagas disease and correlation analyses point
115 to a possible pathogenic role of these cells in the chronic phase of Chagas myocarditis.
116 To our knowledge, the present study is the first to extensively characterize CD4CTLs
117 generated in response to a protozoan pathogen and to elucidate a central mechanism that
118 accounts for their expansion/survival. It is expected that pharmacological targeting of
119 the IL-18R/MyD88 signaling pathway might contribute to the strategic development of
120 new therapeutic and vaccine approaches aiming the control of the CD4CTL response.
121

122 **Results:**

123 ***$CD4^+$ T cells with cytolytic phenotype are abundantly present in the spleen of mice***
124 ***infected with T. cruzi***

125 CD4CTLs express granzyme B (GzB) and perforin (PRF), which are major
126 constituents of CD8CTL and NK cell-granules that promote target cell death in a
127 number of ways (Afonina et al., 2010). Here, we revealed the presence of a
128 TCR$\alpha\beta^+$CD8α^-NK1.1$^-$CD4$^+$GzB$^+$ T cell population, which represents around 30% of
129 CD4$^+$ T cells in the spleen of C57BL/6 (B6) mice, in the acute phase of infection with
130 *T. cruzi* **(Figures 1A-1B)**. Equivalent percentages of CD4$^+$PRF$^+$ T cells were found
131 (**Figure 1C)** and the majority of CD4$^+$GzB$^+$ T cells express PRF and the cytolytic
132 marker 2B4 (CD244) (**Figures 1D-1E** and Figure 1-figure supplement 1A). Of note,
133 most CD4$^+$GzB$^+$ T cells (> 80%) do not express IFN-γ at day 14 post-infection (pi), the
134 peak time-point of the T cell response, and although CD4$^+$GzB$^+$ and CD4$^+$IFN-γ$^+$ cells
135 develop similar kinetics in the spleen, the absolute number of CD4$^+$GzB$^+$ T cells was
136 superior to that of CD4$^+$IFN-γ$^+$ cells, at every time point of infection (**Figures 1F-1G**).
137 It is known that intracellular parasitism by *T. cruzi* Y strain in the spleen is at its highest
138 point between day 12 and 15 pi, concomitant with the histologically observed massive
139 destruction of parasitized splenic macrophages (Cordeiro et al., 1997). Therefore, there
140 is a coincidence between parasite titers in the spleen and the frequency and absolute
141 numbers of CD4$^+$GzB$^+$ T cells. We also observed an increase in the percentage of
142 degranulating CD4$^+$ T cells at day 14 pi, as inferred by staining with anti-CD107a
143 (LAMP-1) mAb, comparable to the observed on CD8$^+$ T cells **(Figure 1H)**, although
144 CD8CTLs are present at higher percentage (Figure 1-figure supplements 1B-E and 1G)
145 and absolute number (Figure 1-figure supplements 1F and 1H). In summary, these data
146 show the remarkable induction of CD4$^+$ T cells with cytolytic potential during infection
147 with *T. cruzi*, an effector subpopulation whose appearance in the spleen parallels and
148 largely outnumbers that of classic GzB-negative IFN-γ$^+$ Th1 cells.

149 ***CD4$^+$ T cells from infected spleen exert Ag-specific cytotoxicity***

150 To ascertain the presence of CD4$^+$ T lymphocytes with cytolytic function, we
151 performed a redirected cytotoxicity assay, where anti-CD3 mAb–coated B cell blasts
152 were used as target cells and co-incubated with either highly purified effector (CD44^{hi})
153 CD4$^+$ T cells sorted from the spleen of infected mice, or naive (CD44^{lo}) CD4$^+$ T cells
154 from non-infected controls. The CTL activity was observed only when effector CD4$^+$ T
155 cells were employed (**Figure 2A**). Antigen-specific cytotoxicity using highly purified
156 CD4$^+$ T cells was also assayed *in vitro* against an I-A^{b+} macrophage cell line (IC-21),
157 loaded or not with *T. cruzi* amastigote total protein extract. Results shown in **Figure 2B**
158 demonstrate that CD4CTLs with cognate cytotoxic activity are present in the spleens of
159 infected mice. The FasL molecule is expressed on CD8$^+$ and CD4$^+$ T cells at the
160 immunological synapse following Ag-triggered degranulation and participates in
161 CD4CTL-mediated lysis of target cells (Bossi & Griffiths, 1999; Brown et al., 2009;
162 Kotov et al., 2018). As shown in **Figure 2B,** addition of anti-FasL mAb to the assay
163 significantly inhibited the specific lysis of target cells, evidentiating the involvement of
164 the FasL/Fas pathway in the killing process.

165 Then, we tested the *in vivo* killing of target splenocytes loaded with class II-
166 restricted peptides (SA85-1.1c and d), derived from a protein of the *T. cruzi*
167 transialidase superfamily (Millar & Kahn, 2000) (**Figure 2C).** The detailed Ag
168 repertoire of CD4CTLs could not be further assessed because of the scarce definition of
169 parasite-derived CD4 epitopes in the literature. To circumvent this, we infected mice
170 with ovalbumin (OVA)-expressing Y strain trypomastigotes (Y-OVA) (Gomes-Neto et
171 al., 2018) and compared the *in vivo* cytotoxic response against known OVA-derived
172 CD4 and CD8 epitopes: $OVA_{323-339}$ and $OVA_{257-264}$, respectively. As shown in **Figure**
173 **2D**, the same level of specific killing was attained against targets loaded with class I-

174 or class II-restricted OVA peptides. Together, these experiments confirmed the presence
175 of a $CD4^+$ T cell subpopulation with Ag-specific cytolytic function against MHC class
176 II-restricted epitopes in the spleen of mice infected with *T. cruzi.*
177
178 ***$CD4^+GzB^+$ T cells express transcription factors typical of CTLs***
179 We then investigated the expression of transcription factors (TFs) typical of
180 cytotoxic cell subsets, such as $CD8^+$ T cells and Tregs. T-bet and Eomesodermin
181 (Eomes) bind to the promoters of the *Gzmb* and *Prf1* genes (Glimcher et al., 2004;
182 Intlekofer et al., 2005; Pearce et al., 2003) and are expressed in CD4CTLs (Curran et al.,
183 2013; Eshima et al., 2012; Qui et al., 2011). **Figures 2E** and **2F** show that the vast
184 majority of $CD4^+GzB^+$ T cells express T-bet, but do not express FoxP3. In accordance
185 with the cytolytic potential of $CD4^+GzB^+$ T cells in our model, 60% of the $CD4^+GzB^+$ T
186 cells express Eomes, while only a small percentage of GzB-negative $CD4^+$ T cells are
187 $Eomes^+$ (**Figure 2G**). Of note, at day 14 pi, the vast majority of both GzB^+ and GzB-
188 negative $CD4^+$ T lymphocytes are effector/memory cells $CD44^{hi}CD62L^{lo}$ (Figure 2-
189 figure supplement 2).
190 CD4CTLs migrating to the gut gradually stop expressing ThPOK, while acquiring
191 the expression of RUNX3 (Mucida et al., 2013; Reis et al., 2013), which is known to
192 drive the CTL gene program in $CD8^+$ CTLs (Cruz-Guilloty et al., 2009; Egawa et al.,
193 2007). The long-form transcript encoding RUNX3 (*Runx3d*) is also expressed in Th1
194 cells, but not in Th2 or naïve cells (Djuretic et al., 2007). As shown in **Figure 2H**,
195 besides *Runx3d* mRNA, we found that $CD4^+GzB^+$ T cells, sorted from the spleen of
196 tamoxifen-treated and infected GzmbCreER^{T2}/ROSA26EYFP reporter mice (Bannard et
197 al., 2009) (Figure 2-figure supplement 3A), express ThPOK *(Zbtb7b gene)*-coding RNA
198 comparable to naive $CD4^+$ T cells, at day 14 pi, when their number and frequency are

199 at the highest levels in this organ (**Figure 1G**). The absence of CD8α-coding transcripts
200 confirms the purity of sorted $CD4^+GzB^+$ T cells (Figure 2-figure supplement 3B). These
201 data show that $CD4^+GzB^+$ T cells generated in response to infection with *T. cruzi,*
202 besides expressing, cytolytic markers, also express T-bet, Eomes and RUNX3, typical
203 TFs found in cytotoxic T cells.
204
205 ***$CD4^+GzB^+$ T cells express cytotoxic markers and immunoregulatory molecules***
206 Tr1 cells are a subset of IL-10-producing $CD4^+FoxP3^-$ T cells that express GzB and
207 PRF and exert a potent suppressive function both in humans and mice (Roncarolo et al.,
208 2018). Since a high percentage of $CD4^+GzB^+$ T cells in our system express Eomes,
209 which drives the development of Tr1 cells (Zhang et al., 2017), we investigated whether
210 *T. cruzi*-induced $CD4^+GzB^+$ T cells would share other phenotypic characteristics with
211 Tr1 cells. We detected a very low frequency of IL-10-producing $TCR\alpha\beta^+CD4^+$ T cells
212 in the spleens of mice infected with *T. cruzi*, in agreement with previous data (Jankovic
213 et al., 2007), although $IL\text{-}10^+$ cells were found to be more frequent among $CD4^+GzB^+$ T
214 cells (**Figures 3A** and Figure 3-figure supplement 1A-B). The co-expression of Lag-3
215 and CD49b was described to define both human and mouse Tr1 cells (Gagliani et al.,
216 2013). Although most splenic $CD4^+GzB^+$ T cells express Lag3, only a minor percentage
217 of these cells co-express CD49b (**Figures 3B-3C** and Figure 3-figure supplement 1C).
218 On the other hand, a substantial fraction of splenic $CD4^+GzB^+$ T cells express the Tim-3
219 immunoregulatory molecule and downregulate CD27 (**Figures 3D-3E**), indicating that
220 these might be terminally differentiated T cells, as suggested in other models (Anderson
221 et al., 2016; Takeuchi & Saito, 2017).
222 Natural killer group 2 (NKG2) members A, C, D and E are C-type lectin-like
223 receptors and cytotoxic markers expressed by NK, NKT, γδ and activated $CD8^+$ T

224 cells (Gunturi et al., 2004; Stojanovic et al., 2018). Recently, NKG2C/E and NKG2D
225 molecules were shown to identify a CD4CTL population, present in mouse lungs during
226 influenza A virus (IAV) infection (Marshall et al., 2017). As shown in **Figures 3F-3G**,
227 the fraction of cells expressing NKG2A/C/E and NKG2D was increased among splenic
228 $CD4^+GzB^+$ T cells, when compared either to GzB-negative $CD4^+$ T cells of infected
229 mice, or with naive $CD4^+$ T cells of non-infected controls (Figure 3-figure supplement
230 2A-B). The class I-restricted T cell associated molecule (CRTAM) was described as
231 being critical to instruct the differentiation of CD4CTLs (Takeuchi et al., 2016;
232 Takeuchi & Saito, 2017). **Figure 3H** shows that the frequency of CRTAM-expressing
233 cells was also increased among splenic $CD4^+GzB^+$ T cells of *T. cruzi*-infected mice,
234 when compared with GzB-negative $CD4^+$ T cells. The frequencies of $CRTAM^+$,
235 $NKG2A/C/E^+$ and $NKG2D^+$ $CD8^+GzB^+$ T cells in infected mice are shown in Figure 3-
236 figure supplement 3. Since at day 14 pi, both GzB^- and GzB^+ $CD4^+$ T cells are in their
237 majority effector/effector memory cells (Figure 2-figure supplement 2), equivalent
238 results were obtained gating on $CD44^{hi}$ cells or not, as shown in Figure 3-figure
239 supplement 4. Together, these results show that a significant fraction of the $CD4^+GzB^+$
240 T cell subpopulation found in this unicellular parasite infection model complies with the
241 general phenotype of CD4CTLs and CD4CTL-precursors reported in response to viral
242 infection.
243
244 ***CD4CTLs are present in lower numbers in Myd88$^{-/-}$ infected mice***
245 To extend our understanding on the requirements for the differentiation of
246 CD4CTLs and their relationship to Th1 cells, we next investigated the role of IL-12,
247 IFN-γ and MyD88 in their generation. IL-12 and IFN-γ are the major cytokines driving
248 Th1 differentiation and T-bet expression, but their requirement for CD4CTL

249 generation is controversial (Brown et al., 2009; Cooper et al., 2004; Curran et al., 2013;
250 Hua et al., 2013; Kotov et al., 2018; Krueger et al., 2021; Tagawa et al., 2016; Xie et al.,
251 2010). Here, we observed that *Il12p40*$^{-/-}$ mice infected with *T. cruzi* displayed lower
252 percentages of T-bet^{+}CD4^{+} and IFN-γ^{+}CD4^{+} T cells and exhibited very low levels of
253 CD4^{+}GzB^{+} T cells (**Figure 4A**). Interestingly, in infected *Ifng*$^{-/-}$ mice, despite the lower
254 frequency of T-bet^{+}CD4^{+} T cells, CD4^{+}GzB^{+} T cells attained the same frequencies as
255 observed in the spleens of WT animals (**Figure 4B**). However, absolute numbers of
256 both total CD4^{+} and CD4^{+}GzB^{+} T cells were lower in *Ifng*$^{-/-}$ mice when compared to
257 WT controls. Thus, both IL-12p40 and IFN-γ play important but distinct roles in the
258 differentiation and expansion/survival of CD4^{+}GzB^{+} T cells.

259 The above results obtained in *Il12p40*$^{-/-}$ and *Ifng*$^{-/-}$ mice, together with the fact that
260 *Myd88*$^{-/-}$ mice have lower levels of Th1 cells and are highly susceptible to infection with
261 *T. cruzi* (Campos et al., 2004; Oliveira et al., 2010), prompted us to address the role of
262 MyD88-dependent pathways in the generation of CD4CTLs. Although infected *Myd88*$^{-}$
263 $^{/-}$ mice displayed equivalent absolute numbers and percentages of total splenic CD4^{+} T
264 cells when compared to WT mice (Figure 4-figure supplement 1A), the frequencies and
265 absolute numbers of CD4^{+}GzB^{+} T cells were significantly lower in this mouse strain
266 (**Figures 4C-4E)**. Furthermore, absolute numbers of CRTAM^{+}, NKG2D^{+} and
267 NKG2A/C/E^{+} CD4^{+}GzB^{+} T cells were severely diminished in *Myd88*$^{-/-}$ mice (**Figures**
268 **4C-4E)**. This picture does not result from lower numbers of total activated CD4^{+} T cells
269 in infected *Myd88*$^{-/-}$ mice, as shown by the percentages and absolute numbers of CD44^{hi}
270 cells, which are equivalent to WT animals (Figure 4-figure supplement 2). On the other
271 hand, absolute numbers of CRTAM^{+}, NKG2D^{+} and NKG2A/C/E^{+} CD8^{+}GzB^{+} T cells
272 were not affected in *Myd88*$^{-/-}$ mice (Figure 4-figure supplement 1C-D). Concerning the
273 expression of perforin, both the percentages and absolute numbers of PRF^{+}CD4^{+} T

274 cells were also severely decreased in *Myd88*$^{-/-}$ compared to WT mice (**Figure 4F**). The
275 same was observed when analyzing the frequency and absolute numbers of PRF^{+}CD4^{+}
276 T cells among GzB-expressing cells (**Figure 4G)**. In order to establish to what extent
277 the absence of MyD88 expression would impact on cytotoxicity mediated by CD4^{+} T
278 splenocytes, we sorted activated CD4^{+}CD44^{hi} T cells from both WT and *Myd88*$^{-/-}$
279 infected mice to a high purity level and performed redirected cytotoxicity assay. Lower
280 levels of cytotoxicity were observed when sorted *Myd88*$^{-/-}$ CD4^{+}CD44^{hi} T cells were
281 employed, as compared to assays using equal numbers of sorted WT CD4^{+}CD44^{hi} T
282 cells (**Figure 4H)**. Together, these results demonstrate the important role of MyD88
283 signaling for the establishment of a robust cytotoxic response mediated by CD4CTLs.
284
285 ***T cell-intrinsic IL-18R/MyD88 signaling plays a crucial role in the establishment of a***
286 ***CD4^{+} T cell subpopulation bearing the CD4CTL gene signature***
287 MyD88 deficiency results in lower IL-12 production by APCs (Campos et al., 2004)
288 and this could explain the diminished numbers of CD4CTLs found in infected *Myd88*$^{-/-}$
289 mice. However, we have recently shown that IL-18R/MyD88 signaling intrinsic to
290 CD4^{+} T cells is critical for Th1 cell proliferation and resistance to apoptosis in response
291 to infection with *T.* cruzi (Oliveira et al., 2017). If CD4CTLs herein described share a
292 common early differentiation process with (or derive from) Th1 cells, it is reasonable to
293 expect that besides IL-12 and IFN-γ, T-cell-intrinsic MyD88-dependent signaling would
294 also be important for the generation of a robust CD4CTL response. In order to test this
295 hypothesis, we constructed mix-BM chimeras, in which WT (B6 x B6.SJL) F1 mice
296 were irradiated and reconstituted with a 1:1 mix of WT and *Myd88*$^{-/-}$ BM cells. After
297 reconstitution, mix-BM chimeras were infected with *T. cruzi* and, at day 14 pi, we
298 sorted WT (CD45.1) and *Myd88*$^{-/-}$ (CD45.2) CD44^{+}CD4^{+} T cells to a high purity level

299 for transcriptome analysis. We have then investigated whether the transcriptional
300 signature of CD4CTLs (Donnarumma et al., 2016) was present in sorted $CD4^+$ T
301 splenocytes and to what extent the absence of T-cell intrinsic MyD88-dependent
302 signaling would impact on the acquirement of this transcriptional program. This
303 signature, previously described in the experimental model of Friend virus infection,
304 distinguishes CD4CTLs from other $CD4^+$ T cell subsets, including Th1 and Tfh cells
305 (Donnarumma et al., 2016). Importantly, gene set enrichment analysis (GSEA),
306 comparing the transcriptome of sorted WT and *Myd88*$^{-/-}$ $CD4^+$ T cells, revealed that 51
307 genes of the CD4CTL signature were upregulated in WT $CD4^+$ T cells, while 78 were
308 downregulated in *Myd88*$^{-/-}$ $CD4^+$ T cells (**Figures 5A-5C**). We confirmed, by flow
309 cytometry, the upregulation of Blimp-1 (*Prdm1* gene) TF and of the ecto-nucleotidase
310 CD39 (*Entpd1*) in WT $CD4^+GzB^+$ T cells (**Figures 5D-5E**). Of note, Blimp-1 is
311 required for the cytotoxic function of CD4CTLs (Hua et al., 2013) and CD39 expression
312 level was found to be higher in $CD4^+GzB^+$ T cells than in Tregs (**Figure 5E**).
313 In order to identify the receptor signaling upstream MyD88 responsible for the
314 establishment of a robust CD4CTL response, we further constructed three groups of
315 mix-BM chimeras, by mixing 1:1 WT and (i) *Il1r1*$^{-/-}$, (ii) *Il18ra*$^{-/-}$ or (iii) *Myd88*$^{-/-}$ BM
316 cells. A fourth group of mix-BM chimeras, 1:1 WT(B6):WT (B6.SJL) control was also
317 generated. After infection with *T. cruzi*, the percentages and absolute numbers of GzB^+
318 cells among $CD4^+$ T cells were analyzed in each chimeric group (gate strategy in Figure
319 5-figure supplement 1). **Figure 5F** shows that the lack of IL-18R signaling in T cells,
320 but not of IL-1R, phenocopied the absence of T cell-intrinsic MyD88 signaling,
321 revealing that IL-18R is a critical pathway upstream MyD88 necessary for the
322 establishment of the $CD4^+GzB^+$ T cell population.

323 In order to further consolidate the role of IL-18R signaling in the generation of a
324 strong CD4CTL response, we analyzed the expression of PRF as well as of CRTAM,
325 NKG2D and NKG2A/C/E cytotoxic markers on $CD4^{+}GzB^{+}$ T cells from the spleens of
326 *Il18ra*$^{-/-}$ mice. **Figure 6A** shows that both the frequency and absolute number of
327 $PRF^{+}CD4^{+}$ T cells were significantly diminished in the spleens of infected *Il18ra*$^{-/-}$
328 compared to WT mice. The same was true for PRF-expressing cells among $GzB^{+}CD4^{+}$
329 T lymphocytes (**Figure 6B)**. As observed in infected *Myd88*$^{-/-}$ mice, the frequency of
330 $GzB^{+}CD4^{+}$ T cells and their absolute number were also decreased in infected *Il18ra*$^{-/-}$
331 compared to WT mice (**Figures 6C-6E**). Absolute numbers of $CRTAM^{+}$, $NKG2D^{+}$ and
332 $NKG2A/C/E^{+}$ $GzB^{+}CD4^{+}$ T cells were significantly diminished in *Il18ra*$^{-/-}$ mice, as
333 well, again phenocopying results obtained in *Myd88*$^{-/-}$ mice (**Figures 6C-6E**). The
334 cytotoxic potential of $CD4^{+}$ T splenocytes from *Il18ra*$^{-/-}$ infected animals was also
335 evaluated by performing redirected cytotoxicity assays with equal numbers of
336 $CD4^{+}CD44^{hi}$ T cells purified from infected *Il18ra*$^{-/-}$ or WT mice. Again, as shown for
337 *Myd88*$^{-/-}$$CD4^{+}$ T cells, lower levels of target killing were observed when employing
338 purified *Il18ra*$^{-/-}$$CD4^{+}CD44^{hi}$ T cells as effectors (**Figure 6F**). Collectively, the present
339 data demonstrate that T-cell intrinsic IL-18R/MyD88 signaling support the generation
340 and/or survival of $CD4^{+}$ T cells with cytotoxic potential in response to parasite
341 infection, revealing a parallel between the requirements for the development of robust
342 Th1 and CD4CTL responses.
343
344 ***The adoptive transfer of CD4^{+}GzB^{+} T cells to Il18ra$^{-/-}$ mice increased survival to***
345 ***infection***
346 *In vivo* studies addressing the function of $CD4^{+}GzB^{+}$ T cells have been hampered by
347 the absence of a stable and abundantly expressed surface-marker of cytotoxicity,

348 which would allow purifying these cells alive. To circumvent this, we employed
349 infected and tamoxifen-treated GzmbCreER^{T2}/ROSA26EYFP reporter mice, from
350 whose spleens CD4$^+$EYFP$^+$ (GzB$^+$) cells were highly purified by flow cytometry and
351 adoptively transferred to infected *Il18ra*$^{-/-}$ mice, following the scheme shown in Figure
352 6-figure supplement 1. The *Il18ra*$^{-/-}$ mouse lineage was previously shown to be very
353 susceptible to infection with *T. cruzi* (Oliveira et al., 2017), and display lower numbers
354 of CD4$^+$GzB$^+$ and CD4$^+$PRF$^+$ T cells with cytotoxic potential, as demonstrated above.
355 The transfer of highly purified CD4$^+$GzB$^+$(EYFP$^+$) T cells to *Il18ra*$^{-/-}$ mice significantly
356 extended their survival rate without, however, decreasing the parasite load in the hearts
357 **(Figure 6G).** In a previous work, we have demonstrated that the transfer of total WT
358 CD4$^+$ T cells protects infected *Il18ra*$^{-/-}$ mice, and this property was attributed to Th1
359 cells, which are also diminished in this mouse lineage (Oliveira et al., 2017). Since
360 infected *Ifng*$^{-/-}$ mice have the same frequency of CD4$^+$GzB$^+$ T cells as WT mice in their
361 spleens (**Figure 4B**), we tested whether the adoptive transfer of CD4$^+$ T cells sorted
362 from *Ifng*$^{-/-}$ mice would also be able to provide some degree of protection to *Il18ra*$^{-/-}$
363 mice. As shown in Figure 6-figure supplement 2, indeed, this was the case. Although
364 IFN-γ expression by CD4$^+$ T cells is necessary for decreasing parasitemia (Oliveira et
365 al., 2017), this result indicated that the secretion of IFN-γ by adoptively transferred
366 CD4$^+$ T cells is not absolutely required for increasing the survival time of infected
367 *Il18ra*$^{-/-}$ recipients. Together, these data demonstrate the protective function of the
368 CD4$^+$GzB$^+$ T cell subset against mortality caused by an intracellular parasite, which is
369 independent of decreasing heart parasitism.
370
371 ***The great majority of CD4$^+$ T cells in the infected myocardium express the CD4CTL***

372 ***phenotype and the frequency of CD4$^+$PRF$^+$ T cells correlates with cardiomyopathy in***
373 ***Chagas patients***

374 Previous studies in viral infection models suggested that CD4CTLs are present
375 in tissues where pathogen replication occurs (Marshall et al., 2017; Takeuchi et al.,
376 2016). Since *T. cruzi* heavily infects the heart, we performed intravascular staining with
377 anti-CD4 mAb and demonstrated that tissue-infiltrating CD4$^+$ T cells are abundant in
378 the myocardium of infected mice (Figure 7-figure supplement 1A-B). As shown in
379 **Figures 7A-7B**, CD4$^+$GzB$^+$ T cells infiltrating the cardiac tissue constitute the vast
380 majority of CD4$^+$ T cells. At the peak time-point of parasite load in the heart,
381 CD4$^+$GzB$^+$ T cells in the myocardium express the LAMP-1 degranulation marker at
382 levels comparable to those of CD8$^+$ T cells (**Figures 7C-D** and Figure 7-figure
383 supplement 1C). Importantly, the great majority of heart-infiltrating CD4$^+$GzB$^+$ T cells
384 expresses PRF, as well as the CRTAM and NKG2D cytotoxic markers (**Figure 7E-7F)**.
385 On the other hand, only few CD4$^+$GzB$^+$ T cells express NKG2A/C/E in the
386 myocardium (Figure 7-figure supplement 1D, left), although high percentages of
387 NKG2A/C/E$^+$CD8$^+$GzB$^+$ T cells were found both in the heart (Figure 7-figure
388 supplement 1D, right) and in the spleen (Figure 3-figure supplement 3A) of infected
389 mice.

390 Finally, we investigated the presence of PRF$^+$CD4$^+$ T cells in the circulation of
391 patients infected with *T. cruzi* and suffering from chronic Chagas cardiomyopathy (CC).
392 In order to ascertain the specificity of CD4$^+$ T cells against *T. cruzi*, PBMC from CC
393 patients or from healthy donors (HD) were incubated (or not) with trypomastigote-
394 derived antigens and analyzed for the expression of perforin by flow cytometry (Figure
395 7-figure supplement 2). As shown in **Figures 7G and 7H,** after treatment, both the
396 expression level of PRF (MFI) and the percentage of PRF$^+$CD4$^+$ T cells increased

397 among $CD4^+$ T cells from CC patients, but not from HD controls. Of note, $CD4^+$ T cells
398 expressing PRF were found at higher frequency in CC patients and their level of PRF
399 expression was also higher than the observed in $CD4^+$ T cells of HD (**Figure 7I**). We
400 next performed correlative analyses between the frequency of PRF-expressing $CD4^+$ T
401 cells in PBMC from CC patients and two echocardiographic parameters, usually
402 employed to evaluate cardiac function in CC patients: left ventricular ejection fraction
403 (LVEF) and left atrium diameter. As shown in **Figure 7J,** a clear inverse correlation
404 between the frequency of $CD4^+PRF^+$ T cells and LVEF, as well as a direct correlation
405 between the frequency of these cells and the left atrium diameter was found. These
406 correlations suggest that CD4CTLs may play a pathogenic role in the chronic phase of
407 Chagas disease. Together, data obtained here in CC patients and in the mouse
408 experimental model point to the heart as an important target-organ for $CD4^+$ T cells
409 with cytolytic potential generated in response to infection with *T. cruzi.*
410
411 **Discussion:**
412 Here we show, for the first time, that CD4CTLs are abundantly present in the
413 spleen of mice infected with *T. cruzi* and that cells with CD4CTL phenotype
414 predominate among $CD4^+$ T cells infiltrating the infected cardiac tissue. The expression
415 of LAMP-1 degranulation marker by $CD4^+GzB^+$ T cells in the heart and in the spleen
416 indicates that these cells may play important effector functions in both organs. These
417 data suggest that $CD4^+GzB^+$ T cells with cytotoxic potential are attracted from the
418 spleen to the cardiac tissue and preferentially accumulate there. $CD4^+GzB^+$ T cells
419 present in the *T. cruzi*-infected hearts express PRF, CRTAM and NKG2D cytotoxicity
420 markers, but differently from CD4CTLs found in the lungs of mice infected with IAV
421 (Marshall et al., 2017), do not express NKG2A/C/E molecules. This interesting

422 dissimilarity requires further investigation and could be due to differential regulation
423 exerted by tissue-specific factors or, alternatively, by different innate responses
424 influencing CD4CTL differentiation, which would be distinctly triggered by viral and
425 parasite pathogens.

426 $CD4^+$ T cells purified from the spleen of infected mice killed APCs presenting
427 parasite-derived antigens *in vitro*. *In vivo* Ag-specific cytotoxicity against I-A^b-
428 restricted epitopes was also observed. Killing infected APCs in the spleen would lead to
429 a decrease in the activation of effector T cells, dampening the exuberant immune
430 response against the parasite. Therefore, the action of CD4CTLs may contribute to
431 immunoregulation, avoiding the development of exacerbated immunopathology, which
432 can cause mortality in the acute phase of the infection with *T. cruzi.* Favoring this
433 hypothesis, we showed that the adoptive transfer of $CD4^+GzB^+$ T cells to susceptible
434 *Il18ra*$^{-/-}$ mice, which have lower levels of these cells, significantly increased their
435 survival to infection, without affecting parasite loads. Together with our previous work
436 (Oliveira et al., 2017), the current results point to possible complementary roles of
437 CD4CTL and Th1 cells. Both cell types might be required for survival against infection
438 with *T. cruzi*, working together to establish a balance between the control of parasite
439 load on one side, and dampening of the immunopathology resulting from this process,
440 on the other. This equilibrium is associated with the establishment of the asymptomatic
441 form of chronic infection (Nunes et al., 2018), in which increased levels of $CD4^+GzB^+$
442 T cells have been found in humans (Keesen et al., 2012). In accordance with a putative
443 regulatory role played by $CD4^+GzB^+$ T cells, we showed here that these cells express
444 surface co-inhibitory receptors at particularly high levels, such as Lag-3 and Tim-3, as
445 well as the ecto-ATPase CD39. These immunoregulatory molecules, typically

446 expressed by Treg and Tr1 cells, have been implicated in suppressive function
447 (Anderson et al., 2016; Mascanfroni et al., 2015; Park et al., 2019).

448 Chronic Chagas cardiomyopathy usually develops in around 30% of infected
449 individuals after decades, probably reflecting an imbalance between parasite and host
450 immune response (Nunes et al., 2018). Although the exact mechanism remains to be
451 elucidated, the association of NK, CD8CTL and GzA-expressing $CD4^+$ T cells with the
452 development of chronic carditis has been indicated (Ferreira et al., 2017; Menezes et al.,
453 2012; Nunes et al., 2018). Since CD4CTLs recognize the cognate antigen in the context
454 of MHC class II molecules, the lysis of infected MHC II^+ endothelial cells might trigger
455 immunopathology (Reis et al., 1993). In the present study we found that the frequency
456 of parasite-specific $CD4^+PRF^+$ T cells is increased in the circulation of chronic cardiac
457 patients with Chagas disease (CC) and that PRF expression in $CD4^+$ T cells is higher in
458 the CC group when compared to healthy donors. A correlation between the frequency of
459 PRF^+CD4^+ T cells and two echocardiographic parameters employed for evaluating
460 myocarditis in CC patients was also encountered. It is tempting to speculate that the loss
461 of regulatory function exerted by different $CD4^+$ T cell subsets, including CD4CTLs,
462 might lead to the chronic pathology. Therefore, further studies are necessary for fully
463 defining the role of tissue infiltrating CD4CTLs in Chagas disease. Interestingly,
464 NKG2D, expressed by most CD4CTLs in the heart, can mediate both activating and
465 inhibitory signals (Wensveen et al., 2018). Importantly, a polymorphism in one of the
466 NKG2D ligands, the major histocompatibility complex class I–related chain A gene
467 (MICA) molecule, was associated with left ventricular systolic dysfunction in patients
468 with chronic Chagas myocarditis (Ayo et al., 2015).

469 We have shown here that $CD4^+GzB^+$ T cells originating in response to *T. cruzi*
470 infection largely outnumber IFN-γ-producing $CD4^+$ T cells and that their appearance

471 in the spleen follows the same kinetics of classic Th1 cells, indicating thereby that
472 differentiation of CD4CTLs is not a late event during infection. Of note, more than 60%
473 of $CD4^+GzB^+$ T cells have downregulated CD27 expression in the spleen at day 14 pi, a
474 characteristic of terminally differentiated T cells (Takeuchi & Saito, 2017). We have
475 also shown here that the majority of $CD4^+GzB^+$ T cells express T-bet, Eomes and
476 Blimp-1. Although Eomes seems not to be essential for CD4CTLs in certain studies
477 (Donnarumma et al., 2016; Kotov et al., 2018), it was proposed to be the master
478 regulator for CD4CTLs and Tr1 cells by others (Curran et al., 2013; Eshima et al.,
479 2012; Qui et al., 2011; Zhang et al., 2017). The $CD4^+GzB^+$ T cell population described
480 herein presents some characteristics of Tr1 cells. However, we only detected a very low
481 frequency of $CD4^+GzB^+$ T cells co-expressing Lag-3 and CD49b (Gagliani et al., 2013)
482 or IL-10. In this regard, data from *T. cruzi* infection differs from those observed during
483 infection with other intracellular parasites such as *T. gondii* and certain *L. major* strains,
484 in which high frequencies of $CD4^+$ T cells producing both IL-10 and IFN-γ were
485 described (Anderson et al., 2007; Jankovic et al., 2007). In contrast with ThPOK-
486 negative CD4CTLs that accumulate in the gut (Cheroutre & Husain, 2013; Mucida et al.,
487 2013; Reis et al., 2013), $CD4^+GzB^+$ T cells in the *T. cruzi*-infected spleen express
488 ThPOK at the peak of infection. Interestingly, the absence of ThPOK downregulation
489 was also observed in mouse (Mittal et al., 2018) and human CD4CTLs (Serroukh et al.,
490 2018). Thus, different subsets of CD4CTL possibly exist, in which the interplay
491 between ThPOK and RUNX3 expression might be differentially regulated.

492 Although many authors consider CD4CTLs merely functional variants of Th1 cells,
493 in some models CD4CTLs fail to fit Th1-defining criteria, such as the dependence on
494 IL-12, STAT4 or T-bet for differentiation (Brown et al., 2009; Curran et al., 2013; Hua
495 et al., 2013; Kotov et al., 2018). Nonetheless, in agreement with other studies (Cooper

496 et al., 2004; Krueger et al., 2021; Tagawa et al., 2016; Xie et al., 2010), we showed here
497 that $CD4^+GzB^+$ T cells are scarcely generated in the absence of IL-12p40. Importantly,
498 we demonstrated that the expansion/survival of CD4CTLs also depends on T-cell
499 intrinsic IL-18R/MyD88 signaling, which we have previously shown to induce cell
500 cycling, anti-apoptotic and Th1-signature transcripts (Oliveira et al., 2017). Notably,
501 several genes of the CD4CTL signature, which distinguishes CD4CTLs from Th1 and
502 Tfh cells (Donnarumma et al., 2016), were expressed by WT, but not by *Myd88*$^{-/-}$ $CD4^+$
503 T cells from infected mix-BM chimeras. Therefore, analogous to its action on Th1 cells,
504 we showed here that T-cell intrinsic IL-18R/MyD88 signaling contributes for the
505 reinforcement and/or stabilization of $CD4^+$ T cell commitment into the CD4CTL
506 phenotype. IFN-γ is another key cytokine involved in Th1 differentiation and *Ifng*$^{-/-}$
507 mice are extremely susceptible to infection with *T. cruzi* (Campos et al., 2004).
508 Interestingly, we found no difference in the frequency of $CD4^+GzB^+$ T cells between
509 WT and *Ifng*$^{-/-}$ infected mice, in accordance with a study showing that IFN-γ had no
510 impact on the ability of CD4 effectors to acquire cytolytic activity (Brown et al., 2012).
511 However, both GzB^+ and total $CD4^+$ T-cell numbers were significantly lower in the
512 infected *Ifng*$^{-/-}$ animals, indicating that IFN-γ might also play a role in the
513 expansion/survival of both Th1 and CD4CTLs in our system. It is known that IFN-γ and
514 IL-18R participate in a reciprocal positive feedback loop in Th1 differentiation process:
515 while IFN-γ is required for IL-12-driven upregulation of IL-18R expression (Nakahira
516 et al., 2001; Smeltz et al., 2001), IL-18 is a major IFN-γ-inducing factor. Therefore, the
517 absence of IL-18R upregulation in $CD4^+$ T cells of *Ifng*$^{-/-}$ mice would prevent the
518 expansion of both $CD4^+$ T cell subpopulations. Thus, in *T. cruzi* infection model, IL-12,
519 IFN-γ and IL-18R/MyD88 signaling act as key pathways at early check-points in the

520 generation of $CD4^+GzB^+$ T cells with cytotoxic potential, suggesting that these cells
521 might share common early differentiating steps with the Th1 subset. It is not excluded,
522 however, that different precursors of CD4CTL and Th1 cells might exist (Takeuchi &
523 Saito, 2017). A cartoon summarizing our results and cited works published by others is
524 shown in Figure 7-figure supplement 3. Of note, in humans, the higher production of
525 IL-18 due to gene polymorphisms has been correlated to protection against chronic
526 Chagas cardiomyopathy (Leon Rodriguez et al., 2016; Nogueira et al., 2015).

527 It is possible that differentiation into CD4CTLs could also be influenced by
528 pathogen-derived factors. Very recently, Krueger *et al*. have shown that a subset of IL-
529 12-dependent Th1-derived cytotoxic cells was present in the spleen of *Il18*$^{-/-}$ mice at
530 later stages of infection with *Salmonella enterica* (Krueger et al., 2021). Whether that
531 result was due to compensatory mechanisms, such as the known exacerbated IL-12
532 production by infected *Il18*$^{-/-}$ mice (Monteforte et al., 2000), or to distinct innate
533 responses, differentially induced by phagosomal bacteria and cytoplasmatic parasites,
534 remains to be determined. Of note, other discrepancies between results obtained with
535 *Il18*$^{-/-}$ versus *Il18ra*$^{-/-}$ mouse lineages have been described in different models in the past
536 (Gutcher et al., 2006; Lewis & Dinarello, 2006). It is known that different classes of
537 pathogens can trigger diverse APC responses and, therefore, elicit pathogen-tailored Th
538 programs (Kara et al., 2014; Kiner et al., 2021). Previous works have reported the
539 immunoregulatory action of *T. cruzi*-derived PAMPs on $CD4^+$ T cell activation, either
540 by directly acting as co-stimulatory signals for T cells, or by modulating APC functions
541 (Bellio et al., 1999; DosReis et al., 2002; Medeiros et al., 2007). It would be interesting
542 to test *T. cruzi*-derived molecules on their capacity to favor the generation of CD4CTLs.

543 In summary, the present work is the first to described a CD4CTL subset abundantly
544 present in the *T. cruzi*-infected cardiac tissue, bringing novel pieces to the scenario of

545 the immune response against a major human intracellular parasite. Importantly, our data
546 disclose a mechanistic framework involved in the generation of a robust CD4CTL
547 response, whose control and optimization may provide new therapeutic and vaccination
548 strategies to combat infection with intracellular pathogens and chronic diseases
549 resulting thereof.
550

551 **Materials and Methods**

552 **Mice.** C57BL/6, B6.SJL and F1 (B6 x B6.SJL) mice were from the Universidade
553 Federal Fluminense. *Myd88*$^{-/-}$ mice were generated by Dr. S. Akira (Osaka University,
554 Japan); *Il12p40*$^{-/-}$ and *Ifng*$^{-/-}$ mice were purchased from USP; *Il18ra*$^{-/-}$ and *Il1r1*$^{-/-}$ mice
555 from JAX Mice, USA. GzB reporter mice, GzmbCreER^{T2}/ROSA26EYFP, previously
556 described (Bannard et al., 2009) were obtained from Dr. Ricardo Gazinelli (UFMG, BH,
557 Brazil). Mice were on the C57BL/6 background, except GzmbCreER^{T2}/ROSA26EYFP,
558 which were on mixed Sv129/B6 background and backcrossed to B6 for 5 generations.
559 In each experiment, only male mice of the same age (6- to 8-week-old) were used. Mice
560 were housed at a maximum of 5 animals per cage, in forced-air-ventilated micro-
561 isolation rack system, in a room at 21–23˚C under a 12/12 h light/dark cycle and
562 provided sterilized water and chow ad libitum. All mouse experiments were conducted
563 in accordance with guidelines of the Animal Care and Use Committee of the Federal
564 University of Rio de Janeiro (Comitê de Ética do Centro de Ciências da Saúde CEUA -
565 CCS/UFRJ, license: IMPPG022).

566 **Experimental infection.** Bloodstream trypomastigotes of the Y strain of *T. cruzi* (2 x
567 10^3 cells/0.2 mL) were inoculated intraperitoneally (i.p.). Y-OVA strain trypomastigotes
568 (Gomes-Neto et al., 2018) were obtained from LLC-MK2 infected cultures and 2 x 10^6
569 trypomastigotes (in 0.2 mL PBS) were inoculated i.p. Rare outliers (mice in which

570 the infection was not properly established) were identified by the lower size of the
571 spleen (total cell number) and lower percentage of $GzB^{+}CD8^{+}$ T cells (inferior of 50%)
572 in the spleen. These outlier mice were excluded from all analyses.

573 **Generation of BM chimeras.** Acidic drinking water (pH 2.5-3.0) was given for 8 days
574 to recipient mice prior to irradiation with a lethal single dose of 800 rad (TH780C -
575 Theratronics, Canada). The day after irradiation, BM cells were transferred and mice
576 were treated with neomycin sulfate (2 mg/mL) in the drinking water for 15 days.
577 Marrow was harvested from the femur and tibia of B6.SJL ($CD45.1^{+}$) and B6, *Myd88*$^{-/-}$,
578 *Il1r1*$^{-/-}$ or *Il18ra*$^{-/-}$ ($CD45.2^{+}$) mice. For mixed BM chimeras, $CD45.1^{+}$ and $CD45.2^{+}$ BM
579 cells were transferred in a 1:1 ratio (2 x 10^{6} cells each) to irradiated mice. In all
580 experiments, mice were infected 6 to 8 weeks after cell transfer, when reconstitution
581 was achieved.

582 **Human population.** A total of thirteen volunteers were enrolled in this study. Nine
583 volunteer patients had positive specific serology for *T. cruzi* and displayed the chronic
584 Chagas cardiomyopathy (CC) with right and/or left ventricular dilation, global left
585 ventricular dysfunction, alterations in the cardiac electric impulse generation and
586 conduction upon electrocardiogram, chest x-rays and echocardiography; four
587 individuals displayed negative specific serological tests for Chagas disease and were
588 included as control group (healthy donors, HD). Patients were from Chagas disease
589 endemic regions within Minas Gerais, Brazil, and were evaluated at the outpatient clinic
590 of the Universidade Federal de Minas Gerais. Healthy donors were from Belo
591 Horizonte, which is a non-endemic region for Chagas disease. We excluded from our
592 study individuals with any other chronic inflammatory diseases, diabetes,
593 heart/circulatory illnesses or bacterial infections. All individuals included in this work
594 were volunteers and treatment and clinical care were offered to all patients, as

595 needed, despite their enrollment in this research project. All participants provided
596 written informed consent for participation in the study. This cross-sectional study is part
597 of an extended project evaluating biomarkers of cardiomyopathy development in
598 Chagas disease, which has the approval of the National Committee of Ethics in
599 Research (CONEP#195/2007) and are in accordance with the Declaration for Helsinki.
600 **PBMC flow cytometry.** Peripheral blood samples were collected in heparin tubes.
601 PBMCs were obtained by separating whole blood over Ficoll (Sigma-Aldrich, St.
602 Louis, MO), as previously described (Menezes et al., 2012). Cells were washed and
603 resuspended in RPMI 1640 medium (Gibco, Rockville, MD) supplemented with 5%
604 heat-inactivated AB human serum, antibiotics (penicillin, 200 U/ml; and streptomycin,
605 0.1 mg/mL) and L-glutamine (1 mM) (Sigma-Aldrich) at a concentration of 1 x 10^7
606 cells/mL. Cells from each volunteer were cultured on 96-well plates (Costar, Corning
607 Incorporated, Corning, NY) in 200 μL of medium alone (ctr) or containing 20 μg/mL of
608 trypomastigote antigen (trypo) for 18h. Trypo was obtained from trypomastigotes
609 purified from VERO cell cultures: parasites were washed, freeze-thaw for 3 cycles,
610 followed by 5 cycles of 5 minutes each of sonication using 30 seconds between them.
611 Samples were ultracentrifugated at 5,000g for 60 min, at 4^oC. Supernatants were
612 collected, dialyzed for 24h and protein quantification performed by Bradford method.
613 Cells (2 x 10^5) were incubated with PerCP-anti-CD4 (clone A161A1) antibody
614 (Biolegend) for 15 min at 4°C, washed in phosphate-buffered saline (PBS) containing
615 1% bovine serum albumin (BSA), and fixed by a 20 min incubation with a 2%
616 formaldehyde. After washing with PBS, cells were permeabilized with 0.5% saponin
617 for 15 min and intracellularly stained with PE-anti-perforin (clone B-D48) antibody
618 (Biolegend) for 20 minutes, washed twice with 0.5% saponin solution, resuspended in

619 PBS and analyzed. A minimum of 100,000 gated events from each sample were
620 collected and analyzed using FlowJo software.
621 **Flow cytometry of mouse cells.** Reagents and antibodies: PB-anti-CD45.1, APC-Cy7-
622 anti-CD45.2, FITC- PE- or BV-605-anti-CD4, PE-anti-CD8, PE-Cy7-anti-NK1.1,
623 BV421-anti-TCRβ, PE-anti-2B4, FITC-anti-CD107a, PE-Cy7-anti-CD39, PE-anti-
624 FasL, PE-Cy7-anti-CRTAM, PE-anti-NKG2D, PE-anti-NKG2A/C/E, FITC- or
625 AlexaFluor647-anti-GzB, PE-anti-Eomes, PE- or A647-anti-T-bet, PE-anti-FoxP3,
626 AlexaFluor647-anti-Blimp1 and PE-anti-PRF were used. All mAbs were purchased
627 from Biolegend, BD Biosciences or eBioscience/Thermo Fisher Scientific. Spleen cells
628 were stained after red blood cell lysis with ACK buffer. Hearts were perfused with 20
629 mL of cold PBS, minced into small fragments and treated with collagenase D (1.0
630 mg/mL) and DNAse I (0.1 mg/mL), for 1 hour at 37ºC. Collagenase D, DNAse I,
631 monensin and saponin were purchased from Sigma-Aldrich. Single cell suspensions
632 were incubated with anti-CD16/CD32 (FcR block) for 5 min and then surface stained
633 for 30 min on ice. For IL-10 and IFN-γ intracellular staining, 2 x 10^6 spleen cells were
634 cultured in the presence of PMA (16 nM), ionomycin (0.5 μM), monensin (5 μM) and
635 brefeldin A (3.0 μg/mL) for 4 hours. After staining for surface markers, cells were fixed
636 with paraformaldehyde 1% for 1 h, permeabilized with saponin 0.2% for 20 min and
637 stained with PE-Cy7-anti-IFN-γ mAb and/or PE-anti-IL-10 mAbs (Biolegend). For TF
638 and GzB/PRF staining, the FoxP3 staining buffer kit (eBioscience, ThermoFisher
639 Scientific) was employed. At least 20,000 events gated on $CD4^+$ T cells were acquired.
640 Analytical flow cytometry was conducted with MoFlo (Beckman Coulter/Dako-
641 Cytomation), FacsCanto, FacsCalibur or BD LSRFortessa (BD Bioscience) and data
642 analyzed with Summit V4.3 software (Dako Colorado, Inc).

643 ***In vitro* and *in vivo* cytotoxicity assays.** For redirected cytotoxic assay, sorted B cells
644 ($B220^+$), previously activated by LPS (InvivoGen) for 48 h and then incubated for 1 h
645 with anti-CD3ε antibody (10 µg/mL), were employed as target cells. FACS-sorted naïve
646 ($CD44^{low}CD4^+$) and effector/memory ($CD44^{hi}CD4^+$) T cells were purified from the
647 spleen of non-infected and infected mice, respectively. Sorted T cells were coincubated
648 at different E:T ratios, with 10^4 target B cells in round-bottom microplates (Costar-
649 Corning) for 14 h, at 37ºC in a 5% CO_2 incubator and in triplicates. After incubation,
650 living target cells were quantified by flow cytometry, after staining with propidium
651 iodide at 0.5 µg/ml (Sigma-Aldrich). For *T. cruzi*-specific cytotoxicity assays, $CD4^+$ T
652 cells were obtained from infected B6 mice, at day 14 pi, and purified by FACS sorting
653 (MoFlo cell sorter, Beckman Coulter/Dako-Cytomation). IC-21 macrophage cell
654 lineage (ATCC) were used as targets *in vitro.* For this, IC-21 cells were counted and
655 split into two tubes: half of the target cells were incubated for 45 min at 37º C in 5%
656 CO_2, in RPMI containing *T. cruzi* amastigote protein extract (30 µg/mL) obtained as
657 previously described (Oliveira et al., 2010). Ag-loaded cells were then stained with 2.5
658 µM CFSE ($CFSE^{Hi}$) (Invitrogen, Life Technologies), and control cells with 0.5 µM
659 CFSE ($CFSE^{Low}$) in 5 mL of warm PBS for 10 min at 37º C. After two washes in RPMI
660 1640 (10% FCS), cells were resuspended at a concentration of 2 x 10^5 cells/mL each
661 and mixed at 1:1 ratio ($CFSE^{Hi}$:$CFSE^{Low}$). Purified $CD4^+$ T cells were added at different
662 E:T ratios. Cells were seeded in duplicate to round-bottom 96-well plate in a final
663 volume of 200 µL. After ON incubation, cells were harvested and incubated with 0.5
664 µg/mL of propidium iodide and PI^+ cells were excluded from FACS analysis. The
665 percentage of specific lysis was calculated using the formula: % of specific lysis = 100x
666 [($CFSE^{Low}$ / $CFSE^{Hi}$) ctr − ($CFSE^{Low}$ / $CFSE^{Hi}$) effector] x ($CFSE^{Low}$ / $CFSE^{Hi}$) ctr^{-1}.
667 For *in vivo* cytotoxicity assays, splenocytes from non-infected B6 mice were

668 employed as target cells after being divided in 3 subpopulations and stained with 10.0
669 (High), 2.5 (Int) and 0.625 (Low) μM of CFSE or of CTV (Invitrogen, Life
670 Technologies). $CFSE^{Int}$ and $CFSE^{Low}$ cells were loaded with one of the following
671 peptides: SA85c (SHNFTLVASVIIEEA), SA85d (LVASVIIEEAPSGNT), $OVA_{323-339}$,
672 $OVA_{257-263}$ or PA8 (VNHRFTLV) at 2 μM, all from GenScript, EUA. $CFSE^{Hi}$ cells
673 were not loaded with any peptide and used as internal control. For calculating the
674 percentage of specific lysis, $CFSE^{Hi}$ and $CFSE^{Int}$ (or $CFSE^{Low}$) were gated together in
675 order to constitute 100% of cells. $CFSE^{Hi}$ and $CFSE^{Int}$ (or $CFSE^{Low}$) populations were
676 then individually gated and specific lysis was calculated using the following formula: %
677 of specific lysis = 100x [($CFSE^{Low\ or\ Int}$ / $CFSE^{Hi}$) ctr − ($CFSE^{Low\ or\ Int}$ / $CFSE^{Hi}$)
678 effector] x ($CFSE^{Low\ or\ Int}$ / $CFSE^{Hi}$) ctr^{-1}.
679 **Real time RT-PCR.** RNA was extracted using the RNeasykit (QIAGEN). cDNA was
680 synthesized using the High Capacity cDNA Reverse Transcription Kit (Invitrogen, Life
681 Technologies), following the manufacturer's instructions. Gene expression was
682 analyzed using primers in combination with SYBR Green® on a StepOneReal Time
683 PCR System (Applied Biosystems, Life Technologies). The expression level of the
684 genes of interest was determined relative to the expression of 18S rRNA. Primers:
685 *Runx3* Fwd.: 5'- ACA GCA TCT TTG ACT CCT TCC -3'; *Runx3* Rev.: 5- GTT GGT
686 GAA CAC GGT GAT TG- 3'; *Thpok* Fwd: 5'- ATG GGA TTC CAA TCA GGT CA-
687 3'; *Thpok* Rev.5'- TTCTTC CTA CAC CCT GTG CC -3'; *CD8a* Fwd: 5' - ACT GCA
688 AGG AAG CAA GTG GT – 3'; *CD8a* Rev: 5'-CAC CGC TAA AGG CAG TTC TC-
689 3'; 18S-Fwd.: 5'- GGG CGT GGG GCG GAG ATA TGC - 3' and 18S-Rev.: 5'- CG
690 CGG ACA CGA AGG CCC CAA A -3'. For parasite load quantification, hearts of
691 infected mice were perfused, minced and immediately homogenized in 1.0 ml of 4.0 M
692 Guanidine thiocyanate (SIGMA-Aldrich) containing 8.0 μl/mL of β-mercaptoethanol

693 and processed for DNA extraction. Generation of PCR standards and detection of
694 parasite tissue load by real-time PCR was carried out as described (Oliveira et al.,
695 2017); briefly, primers amplify a repeated satellite sequence of *T. cruzi* DNA of 195
696 base-pairs: TCZ-Fwd.: (5'-GCTCTTGCCCACAAGGGTGC-3') and TCZ-Rev.: (5'-
697 CCAAGCAGCGGATAGTTCAGG-3'). Reactions with TNF-a-Fwd: (5'-
698 CCTGGAGGAGAAGAGGAAAGAGA-3') and TNF-a-Rev.: (5'-
699 TTGAGGACCTCTGTGTATTTGTCAA-3') primers for *Mus musculus* TNF-α gene
700 were used as loading controls.

701 **Gene-expression analysis.** Gene expression data were extracted with GeneSpring
702 software GX 11.0 software using default parameters. Data were then normalized by
703 subtracting the average from all genes from each gene intensity and dividing the result
704 by the standard deviation of all gene intensities (i.e. z-score normalization). Z ratios
705 were calculated as previously described (Cheadle et al., 2003) and used to compare the
706 difference in expression between WT samples and *Myd88*$^{-/-}$ samples. Gene Set
707 Enrichment Analysis (GSEA) (http://www.broadinstitute.org/gsea/index.jsp) was
708 performed on the genes pre-ranked by Z ratios (1,000 permutations and Weighted
709 Enrichment Statistic) using as data set 82 differentially expressed genes of sorted WT
710 and *Myd88*$^{-/-}$CD4^{+} T cells (GEO accession no. GSE57738) (Oliveira et al., 2017); and
711 using as gene set the CD4^{+}GzmB^{+} (CD4CTL) transcriptional signature (159 upregulated
712 genes) previously described (https://www.ebi.ac.uk/ena/data/view/PRJEB14043).

713 **Adoptive CD4^{+} T cell transfer assay.** Eight-week-old male
714 GzmbCreER^{T2}/ROSA26EYFP mice were infected with 2 x 10^{3} trypomastigotes and
715 treated with 4 mg/animal/day of tamoxifen citrate (Sandoz-Novartis) from day 7 to 11
716 pi by gavage. Spleen cells were harvested and treated with ACK for red blood cells lysis
717 at day 13 pi. Alternatively, CD4^{+} T cells were purified from the spleen of non-treated

718 and infected *Ifng*$^{-/-}$ mice. In both cases, spleen cells were labeled with anti-B220, anti-
719 CD11b, anti-NK1.1, anti-γδTCR, anti-CD8 and biotinylated PE-conjugated anti-CD4
720 antibodies for 30 minutes on ice, followed by staining with PE-Cy7-conjugated
721 Streptavidin for 20 min. Residual PE-Cy7^{+} cells were excluded and EYFP^{+}PE^{+}
722 (CD4^{+}GzB^{+} T cells) or PE^{+}CD4^{+} (*Ifng*$^{-/-}$CD4^{+} T cells) were sorted using MoFlo cell
723 sorter (Beckman Coulter/Dako-Cytomation). CD4^{+}GzB^{+} T cells (2.8 x 10^{5} cells/animal)
724 or *Ifng*$^{-/-}$ CD4^{+} T cells (1.3 x10^{6} cells/animal), both presenting purity higher than 98%,
725 were adoptively transferred by *iv* injection into *Il18ra*$^{-/-}$ recipient mice, previously
726 infected with 1 x 10^{3} trypomastigotes (day 7 pi). Control groups of *Il18ra*$^{-/-}$ and *Myd88*$^{-}$
727 $^{/-}$ infected mice received PBS. Survival was accompanied daily.
728 **Statistics.** Statistical analyses were performed using GraphPad Prism version 6 for Mac
729 OS (GraphPad Software, San Diego California USA, www.graphpad.com). Sample
730 sizes were chosen to allow the detection of statistical differences with $p < 0.5$ using
731 Student's *t* test, or the Log-rank (Mantel-Cox) test for mouse survival curves.
732 Correlation analysis employed Pearson correlation test. When comparing two groups,
733 the minimum number was n=3 per group. In some experiments, the number was
734 increased to n= 9 to permit $p < 0.05$ even considering the possibility of a single outlier
735 in a population. Data are expressed as mean $\pm$ SEM and considered statistically
736 significant if *p* values were < 0.05.
737

Acknowledgments:

General: We would like to thank Dr. Ricardo T. Gazzinelli (Fiocruz, MG, Brazil) for enriching discussion and providing GzmbCreER^{T2}/ROSA26EYFP mouse lineage and Dr. Helder I. Nakaya (USP, SP, Brazil) for helping with Bioinformatics Analyses.

Funding. This study was financed in part by the Coordenação de Aperfeiçoamento de Pessoal de Nível Superior - Brasil (CAPES) - Finance Code 001; Fundação Carlos Chagas Filho de Amparo à Pesquisa do Estado do Rio de Janeiro (FAPERJ); Conselho Nacional de Pesquisas (CNPq) and by The National Institute for Vaccine Development and Technology (INCTV-CNPq) and National Institutes of Health (NIH). CDB and LMB received PhD fellowships from CNPq; AG and EGAN received PhD fellowships from CAPES; FBC and AG received PDJ-CNPq fellowships. GM received PIBIC-CNPq fellowship. AN, WOD and MB received PQ fellowship from CNPq; AN and MB received CNE grant from FAPERJ.

The funders had no role in study design, data collection and analysis, decision to publish, or preparation of the manuscript.

Author contributions: ACO, FBC, WOD, AN and MB conceived and designed the experiments. CDB, AG, FBC, LMB, JRL, AG, EGAN ACO, AN and MB performed the experiments. CDB, JFG, FBC, LMB, GAM, ACO, EGAN, WOD, AN and MB analyzed the data. ACO, WOD, AN and MB contributed parasites/ reagents/ mice/materials/analysis tools. MB wrote the paper.

Competing interests: The authors declare no competing financial interests.

763 **References:**

764

765 Afonina, I. S., Cullen, S. P., & Martin, S. J. (2010). Cytotoxic and non-cytotoxic roles
766 of the CTL/NK protease granzyme B. *Immunol Rev, 235*(1), 105-116. doi:
767 10.1111/j.0105-2896.2010.00908.x

768 Anderson, A. C., Joller, N., & Kuchroo, V. K. (2016). Lag-3, Tim-3, and TIGIT: Co-
769 inhibitory Receptors with Specialized Functions in Immune Regulation. *Immunity,*
770 *44*(5), 989-1004. doi: 10.1016/j.immuni.2016.05.001

771 Anderson, C. F., Oukka, M., Kuchroo, V. J., & Sacks, D. (2007). CD4(+)CD25(-
772)Foxp3(-) Th1 cells are the source of IL-10-mediated immune suppression in chronic
773 cutaneous leishmaniasis. *J Exp Med., 204*(2), 285-297. Epub 2007
774 doi:10.1084/jem.20061886.

775 Ayo, C. M., Oliveira, A. P., Camargo, A. V., Mattos, C. C., Bestetti, R. B., & Mattos, L.
776 C. (2015). Association of the Functional MICA-129 Polymorphism With the Severity
777 of Chronic Chagas Heart Disease. *Clin Infect Dis, 61*(8), 1310-1313. doi:
778 10.1093/cid/civ540

779 Bannard, O., Kraman, M., & Fearon, D. T. (2009). Secondary replicative function of
780 CD8+ T cells that had developed an effector phenotype. *Science, 323*(5913), 505-509.

781 Baumann, C., Bonilla, W. V., Fröhlich, A., Helmstetter, C., Peine, M., Hegazy, A. N., .
782 . . Löhning, M. (2015). T-bet- and STAT4-dependent IL-33 receptor expression
783 directly promotes antiviral Th1 cell responses. *Proc Natl Acad Sci U S A, 112*(13),
784 4056-4061. doi: 10.1073/pnas.1418549112

785 Bellio, M., Oliveira, A. C., Mermelstein, C. S., Capella, M. A., Viola, J. P., Levraud, J.
786 P., . . . Mendonca-Previato, L. (1999). Costimulatory action of glycoinositol-
787 phospholipids from Trypanosoma cruzi: increased interleukin 2 secretion and

788 induction of nuclear translocation of the nuclear factor of activated T cells 1. *FASEB*
789 *J., 13*(12), 1627-1636. doi: 10.1096/fasebj.13.12.1627.
790 Ben-Sasson, S. Z., Hu-Li, J., Quiel, J., Cauchetaux, S., Ratner, M., Shapira, I., . . . Paul,
791 W. E. (2009). IL-1 acts directly on CD4 T cells to enhance their antigen-driven
792 expansion and differentiation. *Proc Natl Acad Sci U S A, 106*(17), 7119-7124. doi:
793 10.1073/pnas.0902745106.
794 Bern, Caryn. (2015). Chagas' Disease. *New England Journal of Medicine, 373*(5), 456-
795 466. doi: 10.1056/NEJMra1410150
796 Bossi, G., & Griffiths, G. M. (1999). Degranulation plays an essential part in regulating
797 cell surface expression of Fas ligand in T cells and natural killer cells. *Nat Med, 5*(1),
798 90-96. doi: 10.1038/4779
799 Brien, J. D., Uhrlaub, J. L., & Nikolich-Zugich, J. (2008). West Nile virus-specific CD4
800 T cells exhibit direct antiviral cytokine secretion and cytotoxicity and are sufficient
801 for antiviral protection. *J Immunol, 181*(12), 8568-8575. doi:
802 10.4049/jimmunol.181.12.8568.
803 Brown, D. M., Kamperschroer, C., Dilzer, A. M., Roberts, D. M., & Swain, S. L.
804 (2009). IL-2 and antigen dose differentially regulate perforin- and FasL-mediated
805 cytolytic activity in antigen specific CD4+ T cells. *Cell Immunol, 257*(1-2), 69-79.
806 doi: 10.1016/j.cellimm.2009.03.002
807 Brown, D. M., Lee, S., Garcia-Hernandez Mde, L., & Swain, S. L. (2012).
808 Multifunctional CD4 cells expressing gamma interferon and perforin mediate
809 protection against lethal influenza virus infection. *J Virol, 86*(12), 6792-6803. doi:
810 10.1128/jvi.07172-11
811 Burel, J. G., Apte, S. H., Groves, P. L., Klein, K., McCarthy, J. S., & Doolan, D. L.
812 (2016). Reduced Plasmodium Parasite Burden Associates with CD38+ CD4+ T

813 Cells Displaying Cytolytic Potential and Impaired IFN-gamma Production. *PLoS*
814 *Pathog, 12*(9), e1005839. doi: 10.1371/journal.ppat.1005839
815 Campos, M. A., Closel, M., Valente, E. P., Cardoso, J. E., Akira, S., Alvarez-Leite, J. I.,
816 . . . Gazzinelli, R. T. (2004). Impaired production of proinflammatory cytokines and
817 host resistance to acute infection with Trypanosoma cruzi in mice lacking functional
818 myeloid differentiation factor 88. *J Immunol, 172*(3), 1711-1718. doi:
819 10.4049/jimmunol.172.3.1711.
820 Canaday, D. H., Wilkinson, R. J., Li, Q., Harding, C. V., Silver, R. F., & Boom, W. H.
821 (2001). CD4(+) and CD8(+) T cells kill intracellular Mycobacterium tuberculosis by a
822 perforin and Fas/Fas ligand-independent mechanism. *J Immunol, 167*(5), 2734-2742.
823 doi: 10.4049/jimmunol.167.5.2734.
824 Cheadle, C., Vawter, M. P., Freed, W. J., & Becker, K. G. (2003). Analysis of
825 microarray data using Z score transformation. *J Mol Diagn, 5*(2), 73-81. doi:
826 10.1016/S1525-1578(10)60455-2.
827 Cheroutre, H., & Husain, M. M. (2013). CD4 CTL: living up to the challenge. *Semin*
828 *Immunol, 25*(4), 273-281. doi: 10.1016/j.smim.2013.10.022.
829 Cooper, D., Pride, M. W., Guo, M., Cutler, M., Mester, J. C., Nasar, F., . . . Natuk, R. J.
830 (2004). Interleukin-12 redirects murine immune responses to soluble or aluminum
831 phosphate adsorbed HSV-2 glycoprotein D towards Th1 and CD4+ CTL responses.
832 *Vaccine, 23*(2), 236-246. doi: 10.1016/j.vaccine.2004.05.011
833 Cordeiro, Z. M., Dahia, A. C., & Andrade, Z. A. (1997). Kinetics of Trypanosoma cruzi
834 destruction in the mouse spleen. *Rev Soc Bras Med Trop, 30*(1), 3-9. doi:
835 10.1590/s0037-86821997000100002
836 Cruz-Guilloty, F., Pipkin, M. E., Djuretic, I. M., Levanon, D., Lotem, J., Lichtenheld,
837 M. G., . . . Rao, A. (2009). Runx3 and T-box proteins cooperate to establish the

838 transcriptional program of effector CTLs. *J Exp Med, 206*(1), 51-59. doi:
839 10.1084/jem.20081242
840 Curran, M. A., Geiger, T. L., Montalvo, W., Kim, M., Reiner, S. L., Al-Shamkhani, A.,
841 . . . Allison, J. P. (2013). Systemic 4-1BB activation induces a novel T cell phenotype
842 driven by high expression of Eomesodermin. *J Exp Med, 210*(4), 743-755. doi:
843 10.1084/jem.20121190
844 Djuretic, I. M., Levanon, D., Negreanu, V., Groner, Y., Rao, A., & Ansel, K. M. (2007).
845 Transcription factors T-bet and Runx3 cooperate to activate Ifng and silence Il4 in T
846 helper type 1 cells. *Nat Immunol, 8*(2), 145-153. doi: 10.1038/ni1424.
847 Donnarumma, T., Young, G. R., Merkenschlager, J., Eksmond, U., Bongard, N., Nutt,
848 S. L., . . . Kassiotis, G. (2016). Opposing Development of Cytotoxic and Follicular
849 Helper CD4 T Cells Controlled by the TCF-1-Bcl6 Nexus. *Cell Rep, 17*(6), 1571-
850 1583. doi: 10.1016/j.celrep.2016.10.013
851 DosReis, G. A., Pecanha, L. M., Bellio, M., Previato, J. O., & Mendonca-Previato, L.
852 (2002). Glycoinositol phospholipids from Trypanosoma cruzi transmit signals to the
853 cells of the host immune system through both ceramide and glycan chains. *Microbes*
854 *Infect., 4*(9), 1007-1013. doi: 10.1016/s1286-4579(02)01616-7.
855 Egawa, T., Tillman, R. E., Naoe, Y., Taniuchi, I., & Littman, D. R. (2007). The role of
856 the Runx transcription factors in thymocyte differentiation and in homeostasis of
857 naive T cells. *J Exp Med, 204*(8), 1945-1957. doi: 10.1084/jem.20070133.
858 Eshima, K., Chiba, S., Suzuki, H., Kokubo, K., Kobayashi, H., Iizuka, M., . . .
859 Shinohara, N. (2012). Ectopic expression of a T-box transcription factor,
860 eomesodermin, renders CD4(+) Th cells cytotoxic by activating both perforin- and
861 FasL-pathways. *Immunol Lett, 144*(1-2), 7-15. doi: 10.1016/j.imlet.2012.02.013
862 Fang, M., Siciliano, N. A., Hersperger, A. R., Roscoe, F., Hu, A., Ma, X., . . . Sigal,

863 L. J. (2012). Perforin-dependent CD4+ T-cell cytotoxicity contributes to control a
864 murine poxvirus infection. *Proc Natl Acad Sci U S A, 109*(25), 9983-9988. doi:
865 10.1073/pnas.1202143109
866 Ferreira, L. R., Ferreira, F. M., Nakaya, H. I., Deng, X., Cândido, D. D., de Oliveira, L.
867 C., . . . Cunha-Neto, E. (2017). Blood Gene Signatures of Chagas Cardiomyopathy
868 With or Without Ventricular Dysfunction. *J Infect Dis, 215*(3), 387-395. doi:
869 10.1093/infdis/jiw540
870 Frazer, L. C., Sullivan, J. E., Zurenski, M. A., Mintus, M., Tomasak, T. E., Prantner, D.,
871 . . . Darville, T. (2013). CD4+ T cell expression of MyD88 is essential for normal
872 resolution of Chlamydia muridarum genital tract infection. *J Immunol, 191*(8), 4269-
873 4279.
874 Gagliani, N., Magnani, C. F., Huber, S., Gianolini, M. E., Pala, M., Licona-Limon, P., .
875 . . Roncarolo, M. G. (2013). Coexpression of CD49b and LAG-3 identifies human and
876 mouse T regulatory type 1 cells. *Nat Med, 19*(6), 739-746. doi: 10.1038/nm.3179
877 Glimcher, L. H., Townsend, M. J., Sullivan, B. M., & Lord, G. M. (2004). Recent
878 developments in the transcriptional regulation of cytolytic effector cells. *Nat Rev*
879 *Immunol, 4*(11), 900-911. doi: 10.1038/nri1490
880 Gomes-Neto, J. F., Sartorius, R., Canto, F. B., Almeida, T. S., Dias, A. A., Barbosa, C.
881 D., . . . Bellio, M. (2018). Vaccination With Recombinant Filamentous fd Phages
882 Against Parasite Infection Requires TLR9 Expression. *Front Immunol, 9*, 1173. doi:
883 10.3389/fimmu.2018.01173
884 Gunturi, A., Berg, R. E., & Forman, J. (2004). The role of CD94/NKG2 in innate and
885 adaptive immunity. *Immunol Res, 30*(1), 29-34. doi: 10.1385/ir:30:1:029
886 Gutcher, I., Urich, E., Wolter, K., Prinz, M., & Becher, B. (2006). Interleukin 18-
887 independent engagement of interleukin 18 receptor-alpha is required for

888 autoimmune inflammation. *Nat Immunol, 7*(9), 946-953. doi: 10.1038/ni1377.
889 Haring, J. S., & Harty, J. T. (2009). Interleukin-18-related genes are induced during the
890 contraction phase but do not play major roles in regulating the dynamics or function
891 of the T-cell response to Listeria monocytogenes infection. *Infect Immun, 77*(5),
892 1894-1903. doi: 10.1128/IAI.01315-08.
893 Hua, L., Yao, S., Pham, D., Jiang, L., Wright, J., Sawant, D., . . . Sun, J. (2013).
894 Cytokine-dependent induction of CD4+ T cells with cytotoxic potential during
895 influenza virus infection. *J Virol, 87*(21), 11884-11893. doi: 10.1128/jvi.01461-13
896 Intlekofer, A. M., Takemoto, N., Wherry, E. J., Longworth, S. A., Northrup, J. T.,
897 Palanivel, V. R., . . . Reiner, S. L. (2005). Effector and memory CD8+ T cell fate
898 coupled by T-bet and eomesodermin. *Nat Immunol, 6*(12), 1236-1244. doi:
899 10.1038/ni1268
900 Jankovic, Dragana, Kullberg, Marika C., Feng, Carl G., Goldszmid, Romina S.,
901 Collazo, Carmen M., Wilson, Mark, . . . Sher, Alan. (2007). Conventional T-
902 bet+FoxP3- Th1 cells are the major source of host-protective regulatory IL-10 during
903 intracellular protozoan infection. *J Exp Med, 204*(2), 273. doi: 10.1084/jem.20062175
904 Jellison, E. R., Kim, S. K., & Welsh, R. M. (2005). Cutting edge: MHC class II-
905 restricted killing in vivo during viral infection. *J Immunol, 174*(2), 614-618. doi:
906 10.4049/jimmunol.174.2.614.
907 Joffre, O., Nolte, M. A., Spörri, R., & Reis e Sousa, C. (2009). Inflammatory signals in
908 dendritic cell activation and the induction of adaptive immunity. *Immunol Rev,*
909 *227*(1), 234-247. doi: 10.1111/j.1600-065X.2008.00718.x
910 Juno, J. A., van Bockel, D., Kent, S. J., Kelleher, A. D., Zaunders, J. J., & Munier, C.
911 M. (2017). Cytotoxic CD4 T Cells-Friend or Foe during Viral Infection? *Front*
912 *Immunol, 8*, 19. doi: 10.3389/fimmu.2017.00019

913 Kara, E. E., Comerford, I., Fenix, K. A., Bastow, C. R., Gregor, C. E., McKenzie, D. R.,
914 & McColl, S. R. (2014). Tailored immune responses: novel effector helper T cell
915 subsets in protective immunity. *PLoS Pathog, 10*(2), e1003905. doi:
916 10.1371/journal.ppat.1003905
917 Keesen, T.S.L., Gomes, J.A.S, Fares, R.C.G., de Araújo, F.F, Ferreira, K.S, Chaves,
918 A.T, Rocha, M.O.C, Correa-Oliveira, R. (2012). Characterization of CD4+ cytotoxic
919 lymphocytes and apoptosis markers induced by *Trypanossoma cruzi* infection. *Scand*
920 *J Immunol,* 76(3), 311-319. doi: 10.1111/j.1365-3083.2012.02730.x.
921 Kiner, E., Willie, E., Vijaykumar, B., Chowdhary, K., Schmutz, H., Chandler, J., . . .
922 Benoist, C. (2021). Gut CD4(+) T cell phenotypes are a continuum molded by
923 microbes, not by T(H) archetypes. *Nat Immunol, 22*(2), 216-228. doi:
924 10.1038/s41590-020-00836-7
925 Kotov, D. I., Kotov, J. A., Goldberg, M. F., & Jenkins, M. K. (2018). Many Th Cell
926 Subsets Have Fas Ligand-Dependent Cytotoxic Potential. *J Immunol, 200*(6), 2004-
927 2012. doi: 10.4049/jimmunol.1700420
928 Krueger, P. D., Goldberg, M. F., Hong, S. W., Osum, K. C., Langlois, R. A., Kotov, D.
929 I., . . . Jenkins, M. K. (2021). Two sequential activation modules control the
930 differentiation of protective T helper-1 (Th1) cells. *Immunity, 54*(4), 687-701 e684.
931 doi: 10.1016/j.immuni.2021.03.006
932 LaRosa, D. F., Stumhofer, J. S., Gelman, A. E., Rahman, A. H., Taylor, D. K., Hunter,
933 C. A., & Turka, L. A. (2008). T cell expression of MyD88 is required for resistance to
934 Toxoplasma gondii. *Proc Natl Acad Sci U S A, 105*(10), 3855-3860. doi:
935 10.1073/pnas.0706663105.
936 Leon Rodriguez, D.A., Carmona, F. D., Echeverría, L. E., González, C. I., & Martin, J.
937 (2016). IL18 Gene Variants Influence the Susceptibility to Chagas Disease. *PLOS*

938 *Negl Trop Dis, 10*(3), e0004583. doi: 10.1371/journal.pntd.0004583
939 Lewis, E. C., & Dinarello, C. A. (2006). Responses of IL-18- and IL-18 receptor-
940 deficient pancreatic islets with convergence of positive and negative signals for the
941 IL-18 receptor. *Proc Natl Acad Sci U S A, 103*(45), 16852-16857. doi:
942 10.1073/pnas.0607917103.
943 Marshall, N. B., Vong, A. M., Devarajan, P., Brauner, M. D., Kuang, Y., Nayar, R., . . .
944 Swain, S. L. (2017). NKG2C/E Marks the Unique Cytotoxic CD4 T Cell Subset,
945 ThCTL, Generated by Influenza Infection. *J Immunol, 198*(3), 1142-1155. doi:
946 10.4049/jimmunol.1601297
947 Mascanfroni, I. D., Takenaka, M. C., Yeste, A., Patel, B., Wu, Y., Kenison, J. E., . . .
948 Quintana, F. J. (2015). Metabolic control of type 1 regulatory T cell differentiation by
949 AHR and HIF1-alpha. *Nat Med, 21*(6), 638-646. doi: 10.1038/nm.3868
950 Medeiros, M. M., Peixoto, J. R., Oliveira, A. C., Cardilo-Reis, L., Koatz, V. L., Van
951 Kaer, L., . . . Bellio, M. (2007). Toll-like receptor 4 (TLR4)-dependent
952 proinflammatory and immunomodulatory properties of the glycoinositolphospholipid
953 (GIPL) from *Trypanosoma cruzi. J Leukoc Biol, 82*(3), 488-496. doi:
954 10.1189/jlb.0706478.
955 Menezes, C. A., Sullivan, A. K., Falta, M. T., Mack, D. G., Freed, B. M., Rocha, M. O.,
956 . . . Dutra, W. O. (2012). Highly conserved CDR3 region in circulating
957 CD4(+)Vbeta5(+) T cells may be associated with cytotoxic activity in Chagas disease.
958 *Clin Exp Immunol, 169*(2), 109-118. doi: 10.1111/j.1365-2249.2012.04608.x.
959 Millar, A. E., & Kahn, S. J. (2000). The SA85-1.1 protein of the Trypanosoma cruzi
960 trans-sialidase superfamily is a dominant T-cell antigen. *Infect Immun, 68*(6), 3574-
961 3580. doi: 10.1128/IAI.68.6.3574-3580.2000.
962 Mittal, P., Abblett, R., Ryan, J. M., Hagymasi, A. T., Agyekum-Yamoah, A.,

963 Svedova, J., . . . Adler, A. J. (2018). An Immunotherapeutic CD137 Agonist Releases
964 Eomesodermin from ThPOK Repression in CD4 T Cells. *J Immunol, 200*(4), 1513-
965 1526. doi: 10.4049/jimmunol.1701039
966 Monteforte, Gina M., Takeda, Kiyoshi, Rodriguez-Sosa, Miriam, Akira, Shizuo, David,
967 John R., & Satoskar, Abhay R. (2000). Genetically Resistant Mice Lacking IL-18
968 Gene Develop Th1 Response and Control Cutaneous Leishmania major Infection. *J*
969 *Immunol 164*(11), 5890-5893. doi: 10.4049/jimmunol.164.11.5890
970 Mucida, D., Husain, M. M., Muroi, S., van Wijk, F., Shinnakasu, R., Naoe, Y., . . .
971 Cheroutre, H. (2013). Transcriptional reprogramming of mature CD4(+) helper T
972 cells generates distinct MHC class II-restricted cytotoxic T lymphocytes. *Nat*
973 *Immunol, 14*(3), 281-289. doi: 10.1038/ni.2523.
974 Nakahira, Masakiyo, Tomura, Michio, Iwasaki, Masayuki, Ahn, Hyun-Jong, Bian,
975 Yang, Hamaoka, Toshiyuki, . . . Fujiwara, Hiromi. (2001). An Absolute Requirement
976 for STAT4 and a Role for IFN-γ as an Amplifying Factor in IL-12 Induction of the
977 Functional IL-18 Receptor Complex. *J Immunol, 167*(3), 1306. doi:
978 10.4049/jimmunol.167.3.1306
979 Nogueira, Luciana Gabriel, Frade, Amanda Farage, Ianni, Barbara Maria, Laugier,
980 Laurie, Pissetti, Cristina Wide, Cabantous, Sandrine, . . . Cunha-Neto, Edecio. (2015).
981 Functional IL18 polymorphism and susceptibility to Chronic Chagas Disease.
982 *Cytokine, 73*(1), 79-83. doi: https://doi.org/10.1016/j.cyto.2015.01.037
983 Nunes, M. C. P., Beaton, A., Acquatella, H., Bern, C., Bolger, A. F., Echeverría, L. E., .
984 . . Marin-Neto, J. A. (2018). Chagas Cardiomyopathy: An Update of Current Clinical
985 Knowledge and Management: A Scientific Statement From the American Heart
986 Association. *Circulation, 138*(12), e169-e209. doi: 10.1161/cir.0000000000000599
987 Oliveira, A. C., de Alencar, B. C., Tzelepis, F., Klezewsky, W., da Silva, R. N.,

988 Neves, F. S., . . . Bellio, M. (2010). Impaired innate immunity in Tlr4(-/-) mice but
989 preserved CD8+ T cell responses against *Trypanosoma cruzi* in Tlr4-, Tlr2-, Tlr9- or
990 Myd88-deficient mice. *PLoS Pathog, 6*(4), e1000870. doi:
991 10.1371/journal.ppat.1000870
992 Oliveira, A. C., Gomes-Neto, J. F., Barbosa, C. D., Granato, A., Reis, B. S., Santos, B.
993 M., . . . Bellio, M. (2017). Crucial role for T cell-intrinsic IL-18R-MyD88 signaling in
994 cognate immune response to intracellular parasite infection. *Elife, 6*. doi:
995 10.7554/eLife.30883
996 Park, Young-Jun, Ryu, Heeju, Choi, Garam, Kim, Byung-Seok, Hwang, Eun Sook,
997 Kim, Hun Sik, & Chung, Yeonseok. (2019). IL-27 confers a protumorigenic activity
998 of regulatory T cells via CD39. *Proc Natl Acad Sci U S A,* 116(8):3106-3111. doi:
999 10.1073/pnas.1810254116
1000 Pearce, Erika L., Mullen, Alan C., Martins, Gislâine A., Krawczyk, Connie M.,
1001 Hutchins, Anne S., Zediak, Valerie P., . . . Reiner, Steven L. (2003). Control of
1002 Effector CD8+ T Cell Function by the Transcription Factor Eomesodermin. *Science,*
1003 *302*(5647), 1041. doi: 10.1126/science.1090148
1004 Poholek, A. C. (2021). Tissue-Specific Contributions to Control of T Cell Immunity.
1005 *Immunohorizons, 5*(6), 410-423. doi: 10.4049/immunohorizons.2000103
1006 Qui, H. Z., Hagymasi, A. T., Bandyopadhyay, S., St Rose, M. C., Ramanarasimhaiah,
1007 R., Menoret, A., . . . Adler, A. J. (2011). CD134 plus CD137 dual costimulation
1008 induces Eomesodermin in CD4 T cells to program cytotoxic Th1 differentiation. *J*
1009 *Immunol, 187*(7), 3555-3564. doi: 10.4049/jimmunol.1101244
1010 Reis, B. S., Rogoz, A., Costa-Pinto, F. A., Taniuchi, I., & Mucida, D. (2013). Mutual
1011 expression of the transcription factors Runx3 and ThPOK regulates intestinal CD4(+)
1012 T cell immunity. *Nat Immunol, 14*(3), 271-280. doi: 10.1038/ni.2518.

1013 Reis, D. D., Jones, E. M., Tostes, S., Lopes, E. R., Chapadeiro, E., Gazzinelli, G., . . .
1014 McCurley, T. L. (1993). Expression of major histocompatibility complex antigens and
1015 adhesion molecules in hearts of patients with chronic Chagas' disease. *Am J Trop Med*
1016 *Hyg, 49*(2), 192-200. doi: 10.4269/ajtmh.1993.49.192.
1017 Robinson, D., Shibuya, K., Mui, A., Zonin, F., Murphy, E., Sana, T., . . . O'Garra, A.
1018 (1997). IGIF does not drive Th1 development but synergizes with IL-12 for
1019 interferon-gamma production and activates IRAK and NFkappaB. *Immunity, 7*(4),
1020 571-581. doi: 10.1016/s1074-7613(00)80378-7
1021 Rodrigues, M. M., Oliveira, A. C., & Bellio, M. (2012). The Immune Response to
1022 Trypanosoma cruzi: Role of Toll-Like Receptors and Perspectives for Vaccine
1023 Development. *J Parasitol Res, 2012*, 507874. doi: 10.1155/2012/507874
1024 Roncarolo, M. G., Gregori, S., Bacchetta, R., Battaglia, M., & Gagliani, N. (2018). The
1025 Biology of T Regulatory Type 1 Cells and Their Therapeutic Application in Immune-
1026 Mediated Diseases. *Immunity, 49*(6), 1004-1019. doi: 10.1016/j.immuni.2018.12.001
1027 Schenten, Dominik, Nish, Simone A, Yu, Shuang, Yan, Xiting, Lee, Heung Kyu,
1028 Brodsky, Igor, . . . Medzhitov, Ruslan. (2014). Signaling through the Adaptor
1029 Molecule MyD88 in CD4+ T Cells Is Required to Overcome Suppression by
1030 Regulatory T Cells. *Immunity, 40*(1), 78-90. doi: 10.1016/j.immuni.2013.10.023.
1031 Serroukh, Y., Gu-Trantien, C., Hooshiar Kashani, B., Defrance, M., Vu Manh, T. P.,
1032 Azouz, A., . . . Marchant, A. (2018). The transcription factors Runx3 and ThPOK
1033 cross-regulate acquisition of cytotoxic function by human Th1 lymphocytes. *Elife, 7*.
1034 doi: 10.7554/eLife.30496
1035 Smeltz, R. B., Chen, J., Hu-Li, J., & Shevach, E. M. (2001). Regulation of interleukin
1036 (IL)-18 receptor alpha chain expression on CD4(+) T cells during T helper (Th)1/Th2
1037 differentiation. Critical downregulatory role of IL-4. *J Exp Med, 194*(2), 143-153.

1038 doi: 10.1084/jem.194.2.143
1039 Stojanovic, A., Correia, M. P., & Cerwenka, A. (2018). The NKG2D/NKG2DL Axis in
1040 the Crosstalk Between Lymphoid and Myeloid Cells in Health and Disease. *Front*
1041 *Immunol, 9*, 827. doi: 10.3389/fimmu.2018.00827
1042 Tagawa, T., Albanese, M., Bouvet, M., Moosmann, A., Mautner, J., Heissmeyer, V., . . .
1043 Hammerschmidt, W. (2016). Epstein-Barr viral miRNAs inhibit antiviral CD4+ T cell
1044 responses targeting IL-12 and peptide processing. *J Exp Med, 213*(10), 2065-2080.
1045 doi: 10.1084/jem.20160248
1046 Takeda, K., Tsutsui, H., Yoshimoto, T., Adachi, O., Yoshida, N., Kishimoto, T., . . .
1047 Akira, S. (1998). Defective NK cell activity and Th1 response in IL-18-deficient
1048 mice. *Immunity, 8*(3), 383-390. doi: 10.1016/s1074-7613(00)80543-9.
1049 Takeuchi, A., Badr Mel, S., Miyauchi, K., Ishihara, C., Onishi, R., Guo, Z., . . . Saito, T.
1050 (2016). CRTAM determines the CD4+ cytotoxic T lymphocyte lineage. *J Exp Med,*
1051 *213*(1), 123-138. doi: 10.1084/jem.20150519
1052 Takeuchi, A., & Saito, T. (2017). CD4 CTL, a Cytotoxic Subset of CD4(+) T Cells,
1053 Their Differentiation and Function. *Front Immunol, 8*, 194. doi:
1054 10.3389/fimmu.2017.00194
1055 Wensveen, F. M., Jelencic, V., & Polic, B. (2018). NKG2D: A Master Regulator of
1056 Immune Cell Responsiveness. *Front Immunol, 9*, 441. doi:
1057 10.3389/fimmu.2018.00441
1058 Wilkinson, T. M., Li, C. K., Chui, C. S., Huang, A. K., Perkins, M., Liebner, J. C., . . .
1059 Xu, X. N. (2012). Preexisting influenza-specific CD4+ T cells correlate with disease
1060 protection against influenza challenge in humans. *Nat Med, 18*(2), 274-280. doi:
1061 10.1038/nm.2612
1062 Xie, Y., Akpinarli, A., Maris, C., Hipkiss, E. L., Lane, M., Kwon, E. K., . . . Antony,

1063 P. A. (2010). Naive tumor-specific CD4(+) T cells differentiated in vivo eradicate
1064 established melanoma. *J Exp Med, 207*(3), 651-667. doi: 10.1084/jem.20091921
1065 Zhang, Ping, Lee, Jason S., Gartlan, Kate H., Schuster, Iona S., Comerford, Iain,
1066 Varelias, Antiopi, . . . Hill, Geoffrey R. (2017). Eomesodermin promotes the
1067 development of type 1 regulatory T (T_{R1}) cells. *Sci Immunol, 2*(10), eaah7152. doi:
1068 10.1126/sciimmunol.aah7152
1069

1070 **Figure Legends:**

1071 **Figure 1: $CD4^+GzB^+PRF^+$ T cells are present at high frequency in the spleen of**
1072 **mice infected with *T. cruzi.* (A)** $CD4^+$ T cell gating strategy **(B and C)** Representative
1073 flow-cytometry dot plots of GzB **(B)** or PRF **(C)** staining, gated on $CD4^+$ T cells of
1074 non-infected and infected B6 mice (left) and mean frequency of $CD4^+GzB^+$ (or
1075 $CD4^+PRF^+$) T cells in the spleen (right). **(D)** Representative dot plots of PRF and GzB
1076 expression in $CD4^+$ T cells gated as in (A) and mean frequencies of PFR^+ among GzB^+
1077 $CD4^+$ T cells (isotype controls on Figure 1-figure supplement 1A). **(E)** Representative
1078 histogram of 2B4 (CD244) expression on $CD8^+$ (blue), $CD4^+GzB^+$ (red) or $CD4^+GzB^-$
1079 T cells (pink), and correspondent mean MFI values; **(F)** Representative dot plots of
1080 GzB and IFN-γ staining in gated $CD4^+$ T splenocytes (left), mean frequencies of
1081 $GzB^+IFN\text{-}\gamma^-$ (red), $GzB^+IFN\text{-}\gamma^+$ (purple) and $GzB^-IFN\text{-}\gamma^+$ (blue) subsets among total
1082 $CD4^+$ (center) or gated on $CD4^+GzB^+$ T cells (right). (**G)** Kinetics of the mean
1083 frequency of $CD4^+IFN\text{-}\gamma^+$ (purple) and $CD4^+GzB^+$ (red) (left), and corresponding
1084 absolute numbers (right). **(H)** Frequency of LAMP-1^+($CD107a^+$) cells among
1085 $CD4^+GzB^+$ (red) or $CD8^+GzB^+$ (blue) T cells in the infected spleen. Data obtained from
1086 individually analyzed mice (n=4), at indicated or 14 day pi. Error bars= SEM. ND=
1087 non-detected. *ns*= non-significant; **= $p \leq 0.01$ (Student t test). All data are
1088 representative of 3 or more independent experiments.

1089

1090 **Figure 2: CD4 T cell-mediated Ag-specific cytotoxicity and TF expression by**
1091 **$CD4^+GzB^+$ T cells. (A)** Mean frequencies of dead target cells (B blasts) in redirected
1092 cytotoxicity assay employing sorted naive (blue) or *in vivo* activated (red) $CD4^+$ T cells
1093 as effectors, at different E:T ratios, in triplicates. **(B)** Specific lysis of IC-21
1094 macrophages (T) loaded with amastigote antigens, coincubated with highly purified

1095 $CD4^+$ T cells (E) at the indicated E:T ratios, in the presence of anti-FasL mAb (red) or
1096 isotype control mAb (blue). Mean values of triplicates ± SEM are shown in **(A)** and **(B)**;
1097 *p≤ 0.05 (two-tailed Student t-test). Data are representative of 3 independent
1098 experiments. Gating strategy on Figure 2-figure supplement 1A. (**C and D)** Percentages
1099 of Ag-specific cytotoxicity *in vivo*; bars represent mean values + SEM (error bars) of
1100 individually analyzed mice (n=3) infected with *T. cruzi* Y in **(C)** or Y-OVA strain in
1101 **(D)**; class I-restricted (PA8 or $OVA_{257-264}$) and class II-restricted (SA851.1c+d or
1102 $OVA_{323-339}$) peptides were employed. Data are representative of 2 independent
1103 experiments. Cell survival was measured by flow cytometry (Figure 2-figure
1104 supplement 1B) and specific lysis calculated as described in Methods. (**E and F)**
1105 Representative dot plots of $CD4^+$ T cells (gated as in Figure 1A) and corresponding
1106 mean frequencies of gated subpopulations: **(E)** GzB and FoxP3 staining and **(F)** GzB
1107 and T-bet staining. **(G)** Representative histogram of Eomes expression in $CD4^+$ T
1108 splenocytes of non-infected mice (ctr, gray) and in GzB^- (black) and GzB^+ (red) $CD4^+$ T
1109 cells from infected mice, gated as in Figs. 1A and 1B (left) and mean frequencies of
1110 $Eomes^+$ cells among these different subpopulations (right). All experiments were done
1111 at day 14 pi. Bars represent mean values of non-infected ctr group n=3 or infected
1112 group, n=3 to 5, individually analyzed mice. Error bars= SEM. **(H)** Runx3d and ThPOK
1113 (*Zbtb7b*) mRNA expression estimated by qRT-PCR in $CD4^+EYFP^+$ T cells sorted from
1114 infected and tamoxifen-treated GzmbCreER^{T2}/ROSA26EYFP mice, as described in
1115 Methods and shown in Figure 2-figure supplement 3A; ND = not detected. Data are
1116 representative of 3 independent experiments.
1117
1118 **Figure 3: Expression of IL-10, immunoregulatory molecules and cytotoxic**
1119 **markers by $CD4^+GzB^+$ T cells. (A)** Representative dot plots of IL-10 staining and

1120 mean frequencies of IL-10$^+$ cells among non-infected (ctr, gray) or GzB$^-$ (black) and
1121 GzB$^+$ (red) CD4$^+$ T cells from infected mice. **(B)** Representative histogram of Lag-3
1122 staining and mean frequency of Lag-3$^+$ cells. **(C)** Representative dot plots of Lag-3 and
1123 CD49b staining and mean frequency of different cells subsets. **(D)** Representative
1124 histogram of Tim-3 staining and mean frequency of Tim-3$^+$ cells among different cells
1125 subsets. **(E)** Representative histogram of CD27 staining and mean frequency of CD27$^+$
1126 cells. **(A-E)** CD4$^+$GzB$^+$ T cells gated as in Figures 1A-1B; staining controls in Figure 3-
1127 figure supplement 1. **(F-H)** Representative dot plots and mean frequencies of **(F)**
1128 NKG2A/C/E, **(G)** NKG2D and **(H)** CRTAM expression among gated CD4$^+$ T
1129 splenocytes. All experiments were done at day 14 pi. Non-infected ctr group, n=3;
1130 infected group, n=3 to 5 mice, individually analyzed. Error bars= SEM; *p≤ 0.05;
1131 ***p≤ 0.001; ****p≤ 0.0001 (two-tailed Student t-test). Data are representative of 3
1132 independent experiments. Staining controls are shown on Figure 3-figure supplement 2.
1133
1134 **Figure 4: CD4CTLs are severely reduced in *Myd88*$^{-/-}$ mice. (A-B)** Representative dot
1135 plots of GzB and T-bet staining on gated CD4$^+$ T splenocytes (left panels) and mean
1136 frequencies of T-bet$^+$, IFN-γ$^+$ and GzB$^+$ CD4$^+$ T cells and absolute numbers of
1137 GzB$^+$CD4$^+$ T cells (on the right) from **(A)** WT (B6) and *Il12p40*$^{-/-}$ mice on day 14 pi
1138 and **(B)** WT and *Ifng*$^{-/-}$ mice on day 11 pi. **(C)** Representative dot plots and gating
1139 strategy, **(D)** mean frequencies and **(E)** absolute numbers of GzB$^+$ or NKG2A/C/E$^+$,
1140 NKG2D$^+$ and CRTAM$^+$ cells among GzB$^+$CD4$^+$ T cells in the spleen of WT (blue) and
1141 *Myd88*$^{-/-}$ (red) mice at day 13 pi. Bars represent mean values in each group; n= 5
1142 individually analyzed mice. Error bars= SEM; ns= non-significant; *p≤ 0.05; **p≤
1143 0.01; ****p≤ 0.0001 (Student t-test). Representative dot plots of GzB, NKG2A/C/E,
1144 NKG2D and CRTAM staining on CD4$^+$ T cells from non-infected animals are shown

1145 in Figure 4-figure supplement 1B. **(F-G)** Frequencies (left) and absolute numbers
1146 (right) of PRF^+ cells among $CD4^+$ T cells **(F)** and of PRF^+ cells among GzB^+CD4^+ T
1147 cells **(G)** in the spleen of WT (blue bars) and *Myd88*$^{-/-}$ (red bars) mice. GzB^+CD4^+ T
1148 cells were gated as shown in Figs. 1A, 1B and 1G. Data in **(F)** and **(G)** are compiled
1149 from four independent experiments with n= 3 animals in each group, each symbol
1150 represents an individual analyzed mice. **(H)** Frequency of dead target cells (B cell
1151 blasts) in cytotoxic assay, after 14 h of co-culture with $CD4^+CD44^{hi}$ T cells sorted from
1152 WT (blue line) or *Myd88*$^{-/-}$ (red line) infected mice at day 13 pi. B cells were coated
1153 with anti-CD3 (left) or not (right). Mean of triplicates +/- SEM for each E:T ratio point
1154 are shown. Data are representative of 3 independent experiments.
1155
1156 **Figure 5: The CD4CTL gene program is absent in MyD88-deficient $CD4^+$ T cells.**
1157 **(A)** GSEA performed using pre-ranked list of genes expressed in WT or *Myd88*$^{-/-}$ $CD4^+$
1158 T cells sorted from mix-BM chimeras using the CD4CTL gene signature previously
1159 described as gene set (66). **(B)** Venn diagram of CD4CTL genes upregulated in WT and
1160 downregulated in *Myd88*$^{-/-}$ $CD4^+$ T cells sorted from chimeric mice. **(C)** Heat map of
1161 normalized CD4CTL-signature gene expression in WT or *Myd88*$^{-/-}$ $CD4^+$ T cells sorted
1162 from chimeric mice: values indicate mean Z-score, upregulated genes in red and
1163 downregulated genes in blue. **(D)** Representative histograms of Blimp-1 expression
1164 (right) and mean frequency of Blimp-1^+ splenocytes (left) among total gated $CD4^+$ T
1165 cells from non-infected mice (ctr, gray shaded area and bar) or among $CD4^+GzB^+$ (red
1166 line and bar) or $CD4^+GzB^-$ (black line and bar) from WT infected mice at day 14 pi.
1167 Individually analyzed mice, n=4. Error bars=SEM, data are representative of 2
1168 independent experiments. **(E)** Representative histograms (left and central panel) and
1169 mean MFI values of CD39 expression (right panel) on gated $FoxP3^-$ (gray shaded area

1170 and bar) or FoxP3^{+} (blue line and bar) CD4^{+} T cells from non-infected (ctr) mice (left);
1171 GzB^{-}FoxP3^{-} (black line and bar), GzB^{-}FoxP3^{+} (purple line and bar) or GzB^{+}FoxP3^{-} (red
1172 line and bar) CD4^{+} T cells from infected WT mice (center), at day 14 pi; individually
1173 analyzed mice (n=4), error bars =SEM; data are representative of 4 independent
1174 experiments. **(F)** Mean frequency (left) and absolute numbers (right) of GzB-expressing
1175 cells among CD45.1^{+} (B6.SJL WT) or CD45.2^{+} (B6 WT or KO) CD4^{+} T splenocytes in
1176 mix-BM chimeric mice, at day 14 pi; WT:WT control chimera group, n=3; other
1177 chimera groups, n=6 or 7. Error bars= SEM, *ns*= non-significant, ***p≤ 0.001,****p≤
1178 0.0001 (Student t-test). Gating strategy and representative dot plots are shown in Figure
1179 5-figure supplement 1. Data are representative of 3 independent experiments.
1180
1181 **Figure 6: CD4CTLs are severely reduced in *Il18ra*$^{-/-}$ mice. (A and B)** Frequencies
1182 and absolute numbers of PRF^{+} cells among CD4^{+} T cells **(A)** and of PRF^{+} cells among
1183 GzB^{+}CD4^{+} T cells **(B)** in WT (blue bars) and *Il18ra*$^{-/-}$ (red bars) spleens. Data are
1184 compiled from two independent experiments with n= 4-5 animals in each group, each
1185 symbol represents an individual mouse. **(C)** Representative dot plots of GzB, CRTAM,
1186 NKG2D and NKG2A/C/E staining in WT and *Il18ra*$^{-/-}$ mice. **(D)** Mean frequencies and
1187 **(E)** absolute numbers of GzB^{+} or CRTAM^{+}, NKG2D^{+} and NKG2A/C/E^{+} cells among
1188 CD4^{+} and CD4^{+}GzB^{+} T cells, respectively. **(A-E)** CD4^{+} T cells gated as in Figs. 1A-1D;
1189 n=4 individually analyzed mice in each group; error bars= SEM, *p≤ 0.05, **p≤ 0.01,
1190 ***p≤ 0.001, *ns*= non-significant (Student t-test). Data are representative of 2
1191 independent experiments. **(F)** Frequency of dead target cells (B cell blasts) in cytotoxic
1192 assay, after 14 h of co-culture with CD4^{+}CD44^{hi} T cells sorted from WT (blue line) or
1193 *Il18ra*$^{-/-}$ (red line) infected mice at day 13 pi. B cells were coated with anti-CD3 (left) or
1194 not (right). Mean of triplicates +/- SEM for each E:T ratio point are shown. **(G)**

1195 Survival curve (left) and parasite load in the heart (right) of infected *Il18ra*$^{-/-}$ mice,
1196 adoptively transferred with CD4^{+}GzB^{+} cells at day 7 pi (red curve), or not (black
1197 curve); time-line in Figure 6-figure supplement 1; n=10 mice in each group; p = 0.0277;
1198 survival data are compiled from two independent experiments.
1199
1200 **Figure 7: Cells with CD4CTL phenotype predominate in the cardiac tissue of**
1201 **infected mice and are at higher frequencies in patients with Chagas**
1202 **cardiomyopathy. (A)** Representative dot plots (gated as in Figure 7-figure supplement
1203 1A), and mean frequency of CD8^{+} and CD4^{+} T cells infiltrating the heart of B6 infected
1204 mice at day 14 pi. **(B and C)** Representative dot plot and mean frequency of **(B)** GzB^{+}
1205 and **(C)** LAMP-1^{+} (CD107a^{+}) cells, among gated CD4^{+} T cells infiltrating the infected
1206 heart; ctr= non-infected, ND= non-detected. **(D)** Mean parasite load in the cardiac tissue
1207 at different time points pi, obtained by real-time PCR, of individually analyzed mice as
1208 described in Methods; Data are representative of at least 8 **(A and B)** or 2 **(C and D)**
1209 independent experiments. **(E)** Representative dot plots and mean frequency of
1210 CRTAM^{+} and NKG2D^{+} cells among gated intracardiac CD4^{+}GzB^{+} T cells. DP=
1211 CRTAM^{+} NKG2D^{+} double positive cells. Individually analyzed mice, n= 4; error bars=
1212 SEM; data are representative of 4 independent experiments. **(F)** Representative dot plots
1213 and mean frequency of PFR^{+} and GzB^{+}PFR^{+} cells among intracardiac CD4^{+}GzB^{+} T
1214 cells; data are compiled from two independent experiments with n= 4 or 5 animals in
1215 each group, each symbol represents an individual analyzed mice. **(G)** Intensity of PRF
1216 staining (MFI) in and **(H)** Frequency of PRF^{+} cells among CD4^{+} T cells in PBMCs
1217 from patients with chronic Chagas disease cardiomyopathy (CC; n=10) and healthy
1218 donors (HD; n=4) cultured overnight in medium alone (ctr) or in the presence of
1219 trypomastigote antigens (+trypo); *p≤ 0.05, **p≤ 0.01, *ns*= non-significant; data

1220 analyzed by paired Student t test. **(I)** Frequency of PRF^+ cells among $CD4^+$ T cells from
1221 PBMCs of patients with chronic Chagas disease cardiomyopathy (CC; n=10) and
1222 healthy donors (HD; n=4) cultured ON in the presence of trypomastigote antigens.
1223 Gating strategy and representative dot plots are shown in Figure 7-figure supplement 2.
1224 **(J)** Correlation analysis between the percentage of $CD4^+PRF^+$ T cells among $CD4^+$ T
1225 cells in PBMCs from CC patients and left ventricular ejection fraction (LVEF) (left
1226 panel) or left atrium diameter (right panel); indicated *p* and *r* values were calculated
1227 using Pearson correlation test.

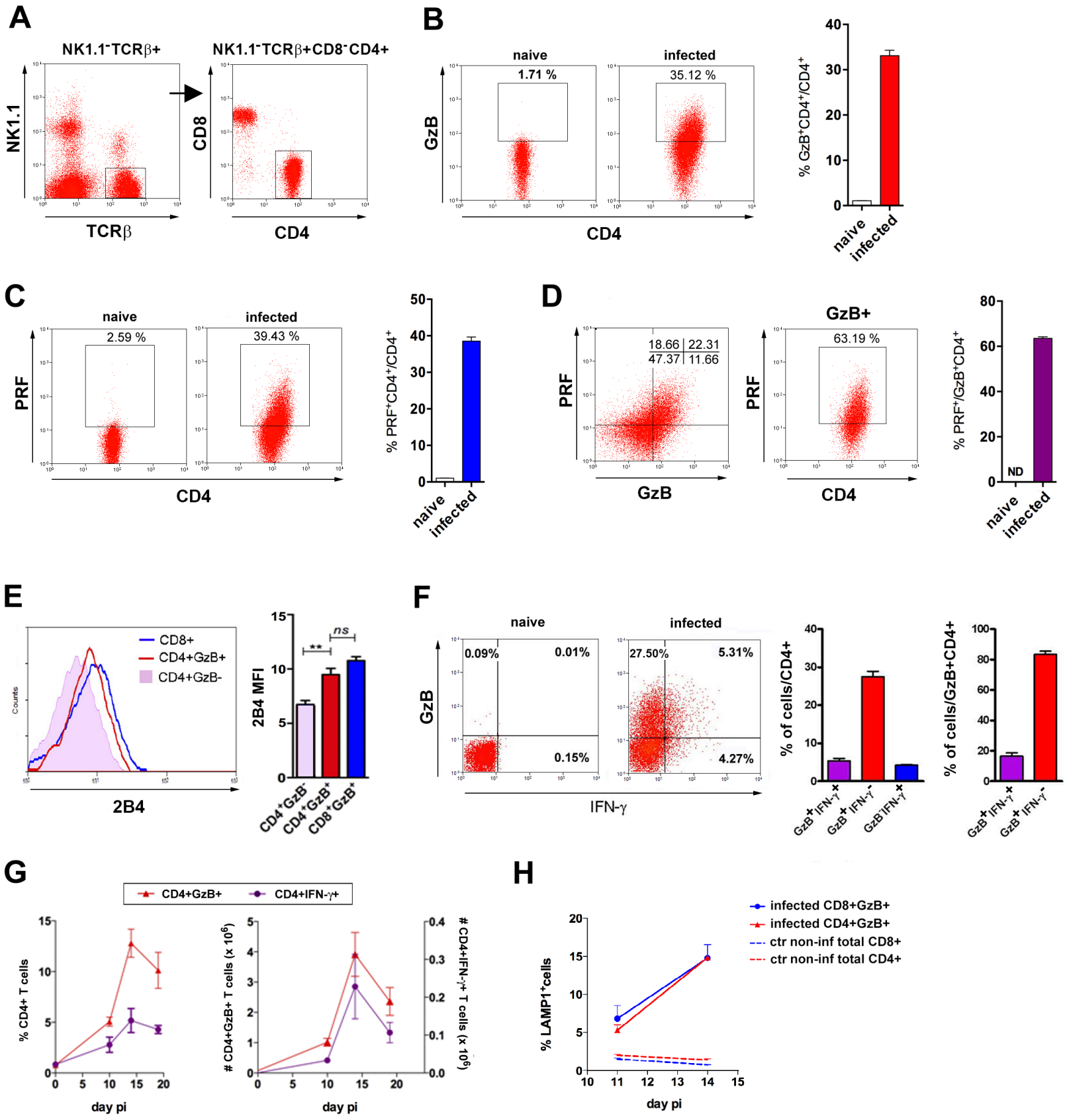
A
NK1.1⁻TCRβ+
NK1.1⁻TCRβ+CD8⁻CD4+
NK1.1
TCRβ
CD8
CD4
B
naive
infected
1.71 %
35.12 %
GzB
CD4
% GzB⁺CD4⁺/CD4⁺
naive
infected
C
naive
infected
2.59 %
39.43 %
PRF
CD4
% PRF⁺CD4⁺/CD4⁺
naive
infected
D
18.66
22.31
47.37
11.66
PRF
GzB
GzB+
63.19 %
PRF
CD4
% PRF⁺/GzB⁺CD4⁺
ND
naive
infected
E
CD8+
CD4+GzB+
CD4+GzB-
Counts
2B4
2B4 MFI
**
ns
CD4⁺GzB⁻
CD4⁺GzB⁺
CD8⁺GzB⁺
F
naive
infected
0.09%
0.01%
0.15%
27.50%
5.31%
4.27%
GzB
IFN-γ
% of cells/CD4+
% of cells/GzB+CD4+
GzB⁺IFN-γ⁺
GzB⁺IFN-γ⁻
GzB⁻IFN-γ⁺
GzB⁺IFN-γ⁺
GzB⁺IFN-γ⁻
G
CD4+GzB+
CD4+IFN-γ+
% CD4+ T cells
# CD4+GzB+ T cells (x 10⁶)
# CD4+IFN-γ+ T cells (x 10⁶)
day pi
day pi
H
infected CD8+GzB+
infected CD4+GzB+
ctr non-inf total CD8+
ctr non-inf total CD4+
% LAMP1⁺cells
day pi

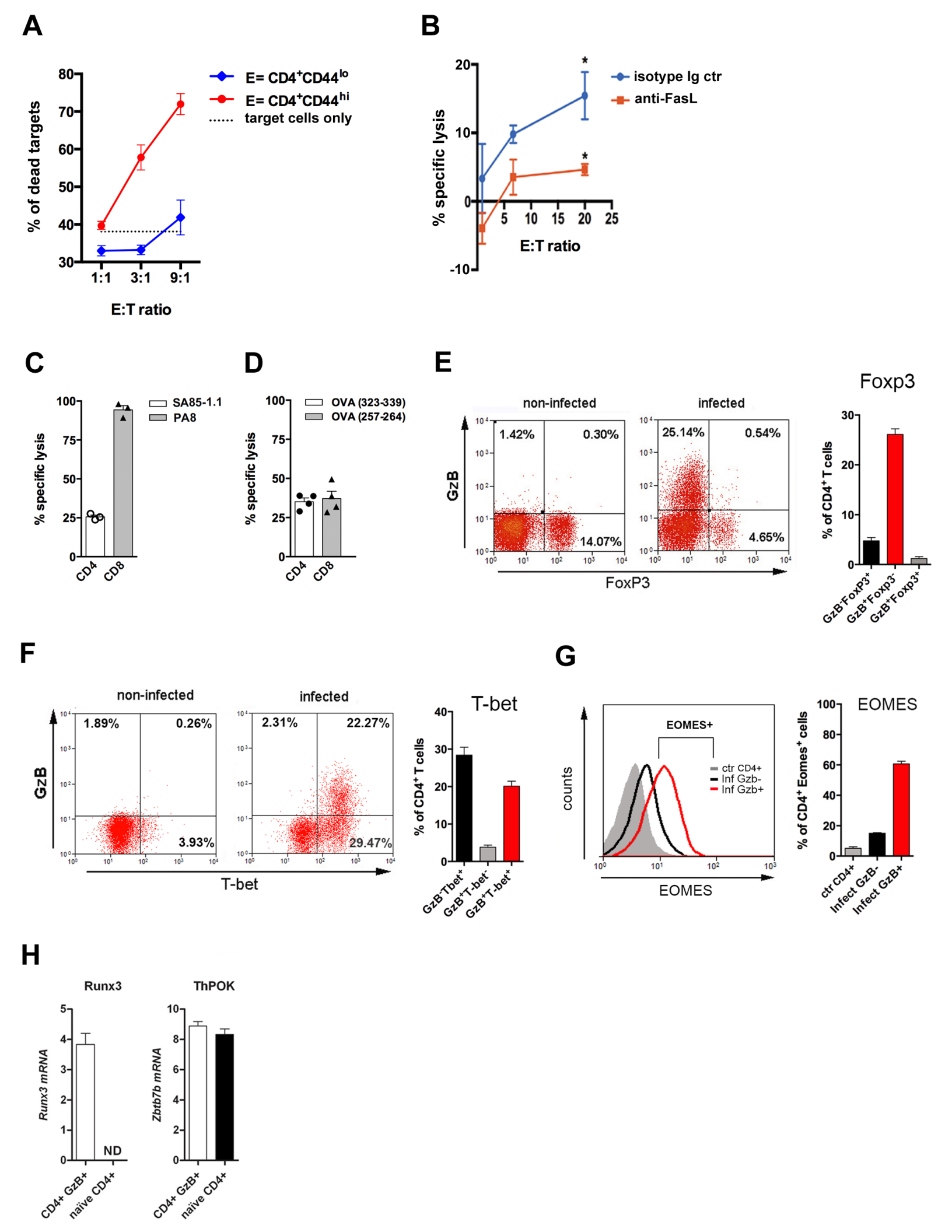
A
% of dead targets
E:T ratio
1:1
3:1
9:1
E= CD4+CD44lo
E= CD4+CD44hi
target cells only
B
% specific lysis
E:T ratio
isotype Ig ctr
anti-FasL
C
% specific lysis
SA85-1.1
PA8
CD4
CD8
D
% specific lysis
OVA (323-339)
OVA (257-264)
CD4
CD8
E
non-infected
infected
GzB
FoxP3
1.42%
0.30%
14.07%
25.14%
0.54%
4.65%
Foxp3
% of CD4+ T cells
GzB-FoxP3+
GzB+Foxp3-
GzB+Foxp3+
F
non-infected
infected
GzB
T-bet
1.89%
0.26%
3.93%
2.31%
22.27%
29.47%
T-bet
% of CD4+ T cells
GzB-Tbet+
GzB+T-bet-
GzB+T-bet+
G
counts
EOMES+
ctr CD4+
Inf Gzb-
Inf Gzb+
EOMES
EOMES
% of CD4+ Eomes+ cells
ctr CD4+
Infect GzB-
Infect GzB+
H
Runx3
ThPOK
Runx3 mRNA
Zbtb7b mRNA
ND
CD4+ GzB+
naïve CD4+
CD4+ GzB+
naïve CD4+

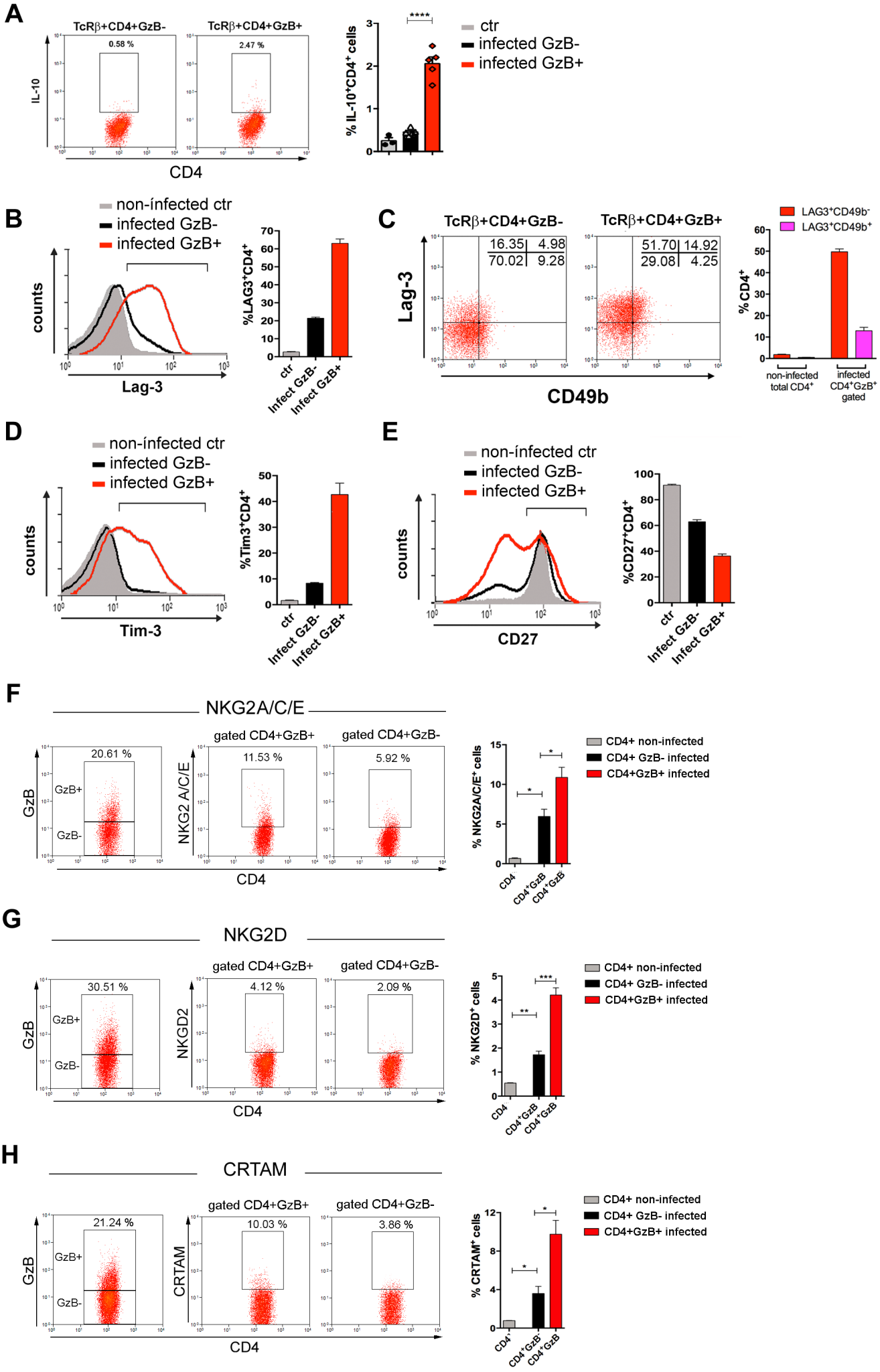
A
TcRβ+CD4+GzB-
TcRβ+CD4+GzB+
0.58 %
2.47 %
IL-10
CD4
% IL-10+CD4+ cells
****
ctr
infected GzB-
infected GzB+
B
non-infected ctr
infected GzB-
infected GzB+
counts
Lag-3
%LAG3+CD4+
ctr
Infect GzB-
Infect GzB+
C
TcRβ+CD4+GzB-
TcRβ+CD4+GzB+
16.35
4.98
70.02
9.28
51.70
14.92
29.08
4.25
Lag-3
CD49b
LAG3+CD49b-
LAG3+CD49b+
% CD4+
non-infected total CD4+
infected CD4+GzB+ gated
D
non-infected ctr
infected GzB-
infected GzB+
counts
Tim-3
%Tim3+CD4+
ctr
Infect GzB-
Infect GzB+
E
non-infected ctr
infected GzB-
infected GzB+
counts
CD27
%CD27+CD4+
ctr
Infect GzB-
Infect GzB+
F
NKG2A/C/E
gated CD4+GzB+
gated CD4+GzB-
20.61 %
11.53 %
5.92 %
GzB
GzB+
GzB-
NKG2 A/C/E
CD4
% NKG2A/C/E+ cells
CD4+ non-infected
CD4+ GzB- infected
CD4+GzB+ infected
CD4-
CD4+GzB-
CD4+GzB+
G
NKG2D
gated CD4+GzB+
gated CD4+GzB-
30.51 %
4.12 %
2.09 %
GzB
GzB+
GzB-
NKGD2
CD4
% NKG2D+ cells
CD4+ non-infected
CD4+ GzB- infected
CD4+GzB+ infected
CD4-
CD4+GzB-
CD4+GzB+
H
CRTAM
gated CD4+GzB+
gated CD4+GzB-
21.24 %
10.03 %
3.86 %
GzB
GzB+
GzB-
CRTAM
CD4
% CRTAM+ cells
CD4+ non-infected
CD4+ GzB- infected
CD4+GzB+ infected
CD4-
CD4+GzB-
CD4+GzB+

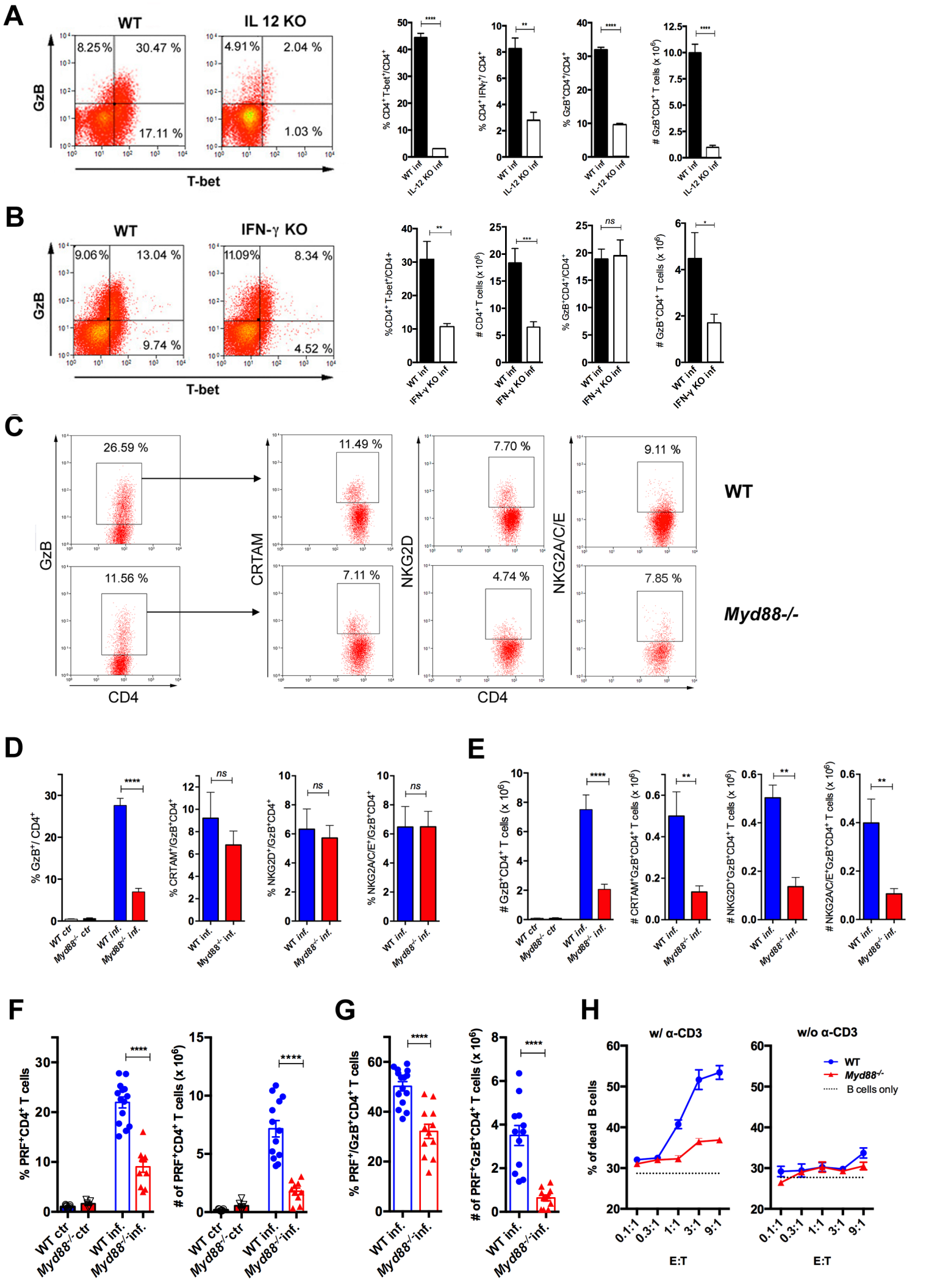
A
WT
IL 12 KO
8.25 %
30.47 %
17.11 %
4.91 %
2.04 %
1.03 %
GzB
T-bet
% CD4+ T-bet+/CD4+
% CD4+ IFNγ+/ CD4+
% GzB+CD4+/CD4+
# GzB+CD4+ T cells (x 10^6)
WT inf
IL-12 KO inf
B
WT
IFN-γ KO
9.06 %
13.04 %
9.74 %
11.09%
8.34 %
4.52 %
%CD4+ T-bet+/CD4+
CD4+ T cells (x 10^6)
IFN-γ KO inf
ns
C
26.59 %
11.56 %
11.49 %
7.11 %
7.70 %
4.74 %
9.11 %
7.85 %
CRTAM
NKG2D
NKG2A/C/E
CD4
WT
Myd88-/-
D
% GzB+/ CD4+
% CRTAM+/GzB+CD4+
% NKG2D+/GzB+CD4+
% NKG2A/C/E+/GzB+CD4+
WT ctr
Myd88-/- ctr
WT inf.
Myd88-/- inf.
E
GzB+CD4+ T cells (x 10^6)
CRTAM+GzB+CD4+ T cells (x 10^6)
NKG2D+GzB+CD4+ T cells (x 10^6)
NKG2A/C/E+GzB+CD4+ T cells (x 10^6)
F
% PRF+CD4+ T cells
# of PRF+CD4+ T cells (x 10^6)
G
% PRF+/GzB+CD4+ T cells
# of PRF+GzB+CD4+ T cells (x 10^6)
H
w/ α-CD3
w/o α-CD3
% of dead B cells
WT
Myd88-/-
B cells only
0.1:1
0.3:1
1:1
3:1
9:1
E:T

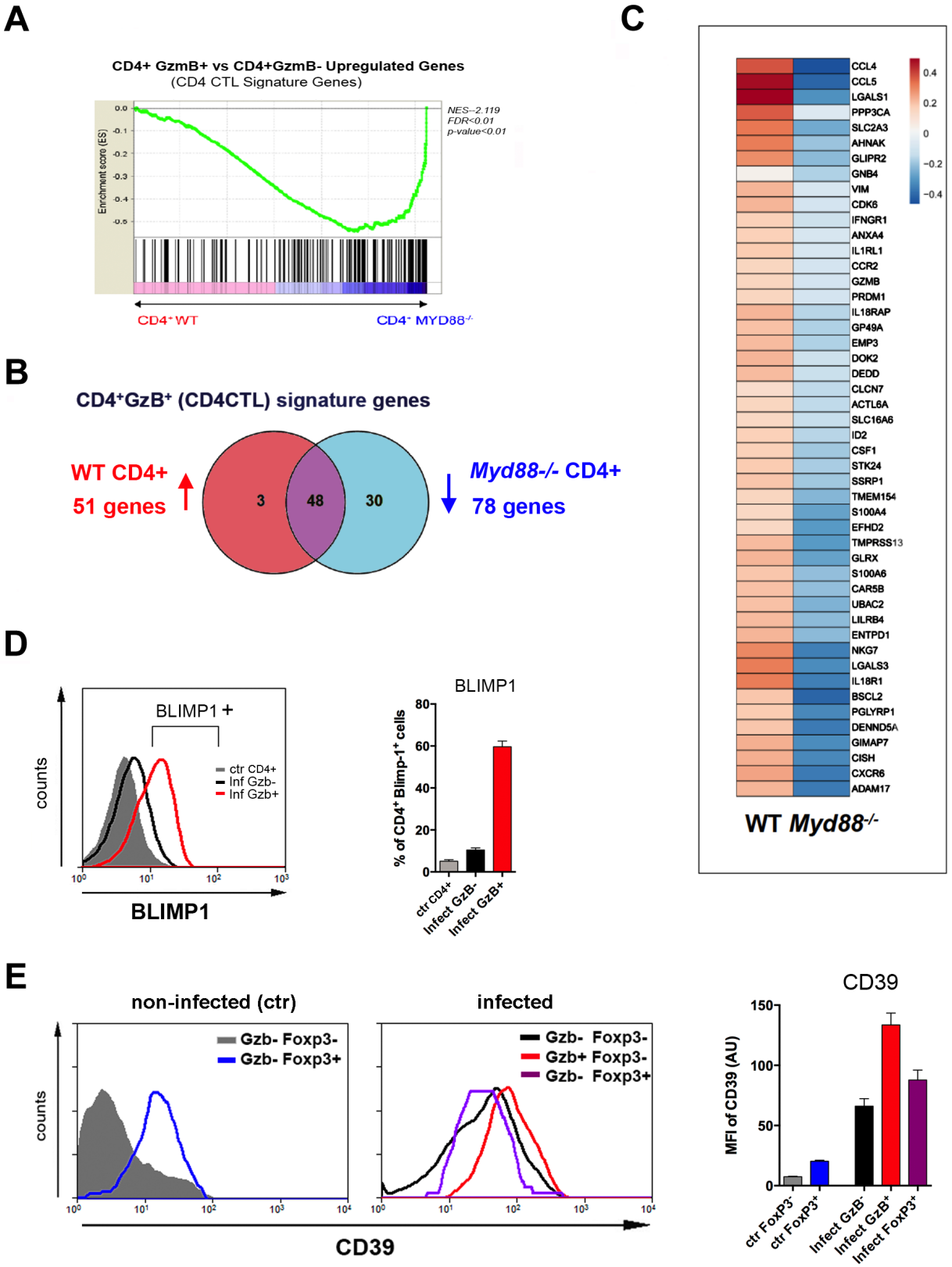
A
CD4+ GzmB+ vs CD4+GzmB- Upregulated Genes
(CD4 CTL Signature Genes)
Enrichment score (ES)
NES=-2.119
FDR<0.01
p-value<0.01
CD4+ WT
CD4+ MYD88-/-
B
CD4+GzB+ (CD4CTL) signature genes
WT CD4+
51 genes
3
48
30
Myd88-/- CD4+
78 genes
C
CCL4
CCL5
LGALS1
PPP3CA
SLC2A3
AHNAK
GLIPR2
GNB4
VIM
CDK6
IFNGR1
ANXA4
IL1RL1
CCR2
GZMB
PRDM1
IL18RAP
GP49A
EMP3
DOK2
DEDD
CLCN7
ACTL6A
SLC16A6
ID2
CSF1
STK24
SSRP1
TMEM154
S100A4
EFHD2
TMPRSS13
GLRX
S100A6
CAR5B
UBAC2
LILRB4
ENTPD1
NKG7
LGALS3
IL18R1
BSCL2
PGLYRP1
DENND5A
GIMAP7
CISH
CXCR6
ADAM17
WT Myd88-/-
D
BLIMP1 +
counts
ctr CD4+
Inf Gzb-
Inf Gzb+
BLIMP1
BLIMP1
% of CD4+ Blimp-1+ cells
ctr CD4+
Infect GzB-
Infect GzB+
E
non-infected (ctr)
infected
counts
Gzb- Foxp3-
Gzb- Foxp3+
Gzb- Foxp3-
Gzb+ Foxp3-
Gzb- Foxp3+
CD39
CD39
MFI of CD39 (AU)
ctr FoxP3-
ctr FoxP3+
Infect GzB-
Infect GzB+
Infect FoxP3+
F
%CD4+GzB+/CD4+
ctr
inf
WT: WT
WT: Myd88
WT: Il1r
WT: Il18r
****
ns
***
# of CD4+GzB+(x 10^6)
WT (CD45.1+)
WT (CD45.2+)
Myd88-/- (CD45.2+)
Il1r-/- (CD45.2+)
Il18r-/- (CD45.2+)

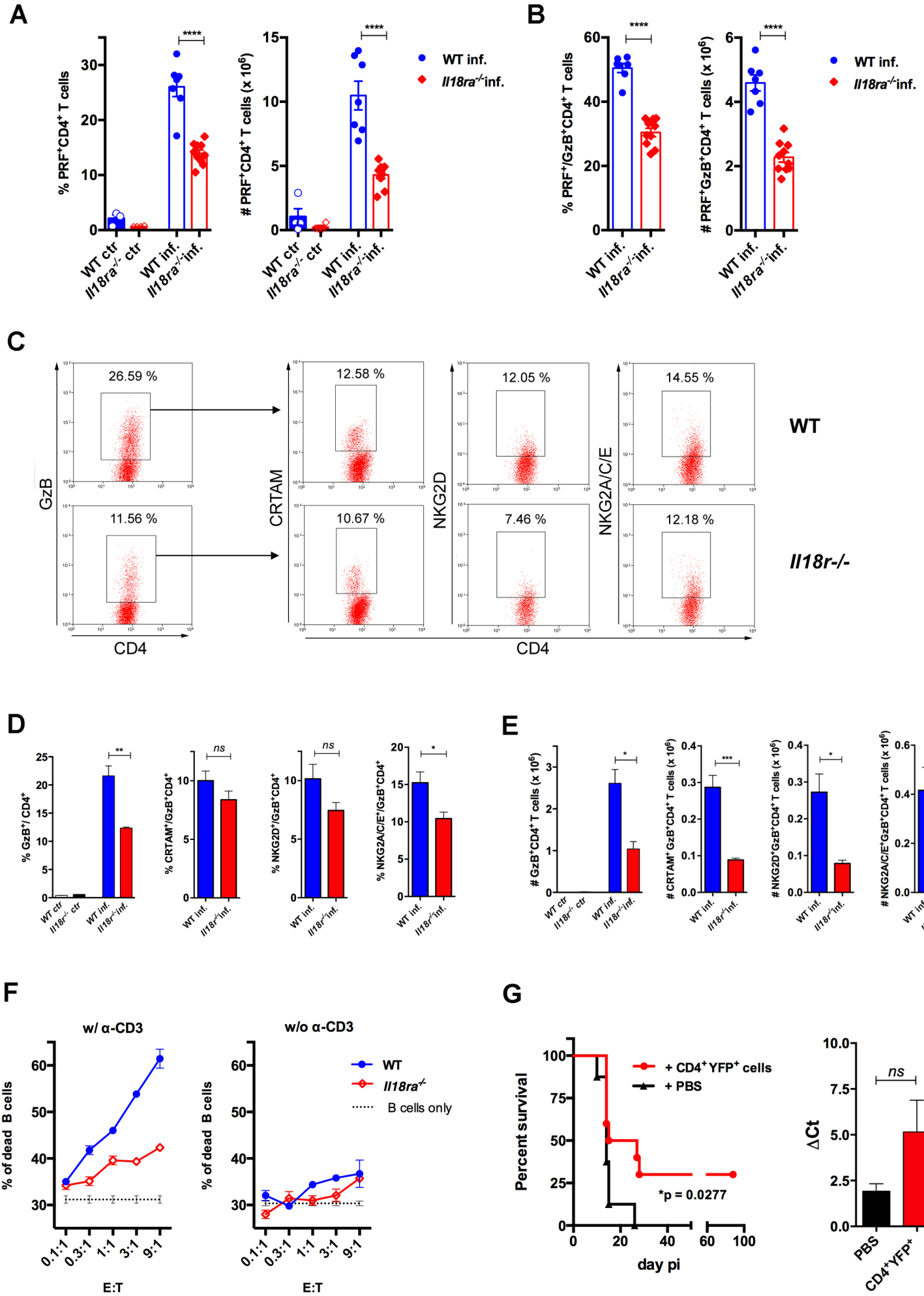
A
% PRF+CD4+ T cells
# PRF+CD4+ T cells (x 10^6)
****
WT inf.
Il18ra-/-inf.
WT ctr
Il18ra-/- ctr
WT inf.
Il18ra-/-inf.
B
% PRF+/GzB+CD4+ T cells
# PRF+GzB+CD4+ T cells (x 10^6)
C
26.59 %
11.56 %
12.58 %
10.67 %
12.05 %
7.46 %
14.55 %
12.18 %
GzB
CRTAM
NKG2D
NKG2A/C/E
CD4
WT
Il18r-/-
D
% GzB+/ CD4+
% CRTAM+/GzB+CD4+
% NKG2D+/GzB+CD4+
% NKG2A/C/E+/GzB+CD4+
**
ns
*
E
GzB+CD4+ T cells (x 10^6)
CRTAM+ GzB+CD4+ T cells (x 10^6)
NKG2D+GzB+CD4+ T cells (x 10^6)
NKG2A/C/E+GzB+CD4+ T cells (x 10^6)
***
F
w/ α-CD3
w/o α-CD3
% of dead B cells
WT
Il18ra-/-
B cells only
0.1:1
0.3:1
1:1
3:1
9:1
E:T
G
Percent survival
+ CD4+ YFP+ cells
+ PBS
*p = 0.0277
day pi
ΔCt
ns
PBS
CD4+YFP+

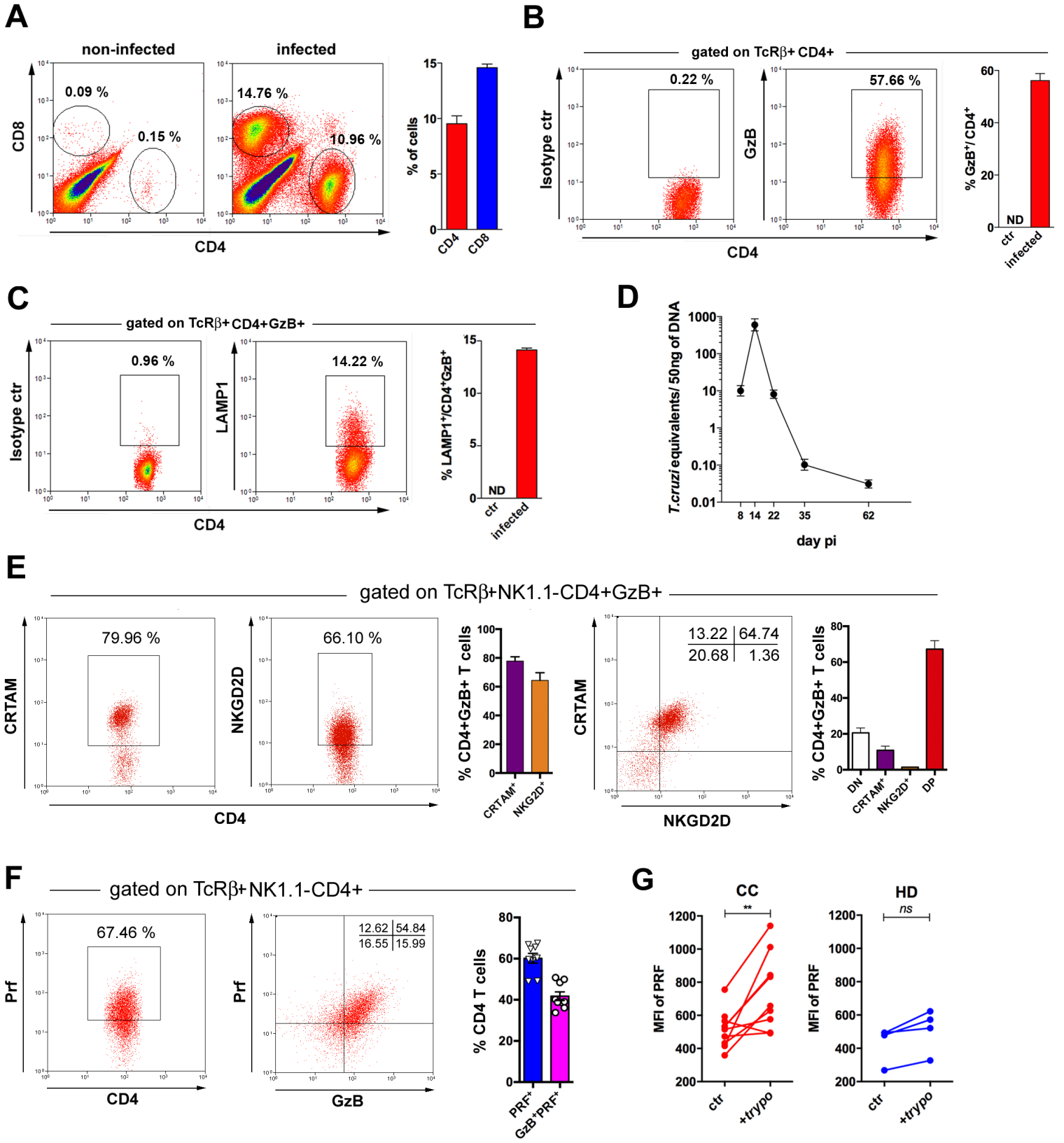
A
non-infected
infected
CD8
CD4
0.09 %
0.15 %
14.76 %
10.96 %
% of cells
CD4
CD8
B
gated on TcRβ+ CD4+
Isotype ctr
GzB
0.22 %
57.66 %
% GzB+/CD4+
ND
ctr
infected
C
gated on TcRβ+CD4+GzB+
Isotype ctr
LAMP1
0.96 %
14.22 %
% LAMP1+/CD4+GzB+
D
T.cruzi equivalents/ 50ng of DNA
day pi
E
gated on TcRβ+NK1.1-CD4+GzB+
CRTAM
NKGD2D
79.96 %
66.10 %
% CD4+GzB+ T cells
13.22
64.74
20.68
1.36
DN
DP
F
gated on TcRβ+NK1.1-CD4+
Prf
67.46 %
12.62
54.84
16.55
15.99
% CD4 T cells
PRF+
GzB+PRF+
G
CC
HD
ns
MFI of PRF
ctr
+trypo
H
% PRF+CD4+ T cells
I
J
LVEF%
p= 0.04
r= -0.62
Left atrium (mm)
p= 0.05
r= 0.80
% PRF+ CD4+ T cells

SUPPLEMENTAL MATERIAL

Cytotoxic CD4$^+$ T cells driven by T-cell intrinsic IL-18R/MyD88 signaling predominantly infiltrate *Trypanosoma cruzi*-infected hearts

Carlos-Henrique. D. Barbosa[1,2], Ariel Gomes[1,3], Fábio B. Canto[1,4], Layza M. Brandão[1], Jéssica R. Lima[1], Guilherme A. Melo[1], Alessandra Granato[1,5], Eula G.A. Neves[6], Walderez O. Dutra[6], Ana C. Oliveira[7], Alberto Nóbrega[1] and Maria Bellio[1]*.

**corresponding author.*
e-mail: belliom@micro.ufrj.br or mariabellioufrj@gmail.com

Supplemental Figures.

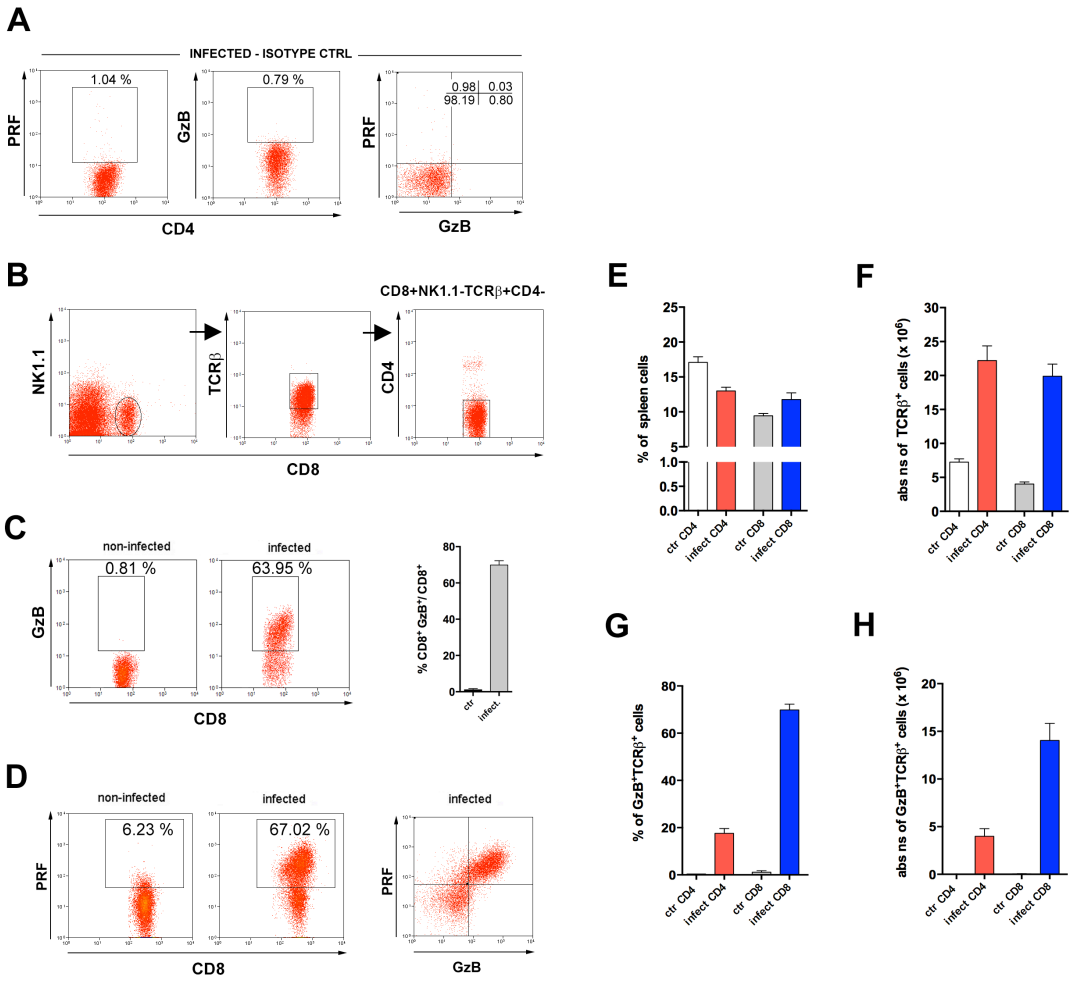

Figure 1–figure supplement 1: Comparative percentages and absolute numbers of GzB$^+$ and PRF$^+$ T cell subsets. (A) Isotype control staining of CD4$^+$ T cells, gated as in Fig. 1A, from infected mice. **(B)** Gating strategy for **C** and **D** plots. **(C)** Representative dot plots of GzB staining and mean frequency of GzB$^+$CD8$^+$T cells (on the right). **(D)** Representative dot plots of PRF and GzB staining in CD8$^+$ T cells. **(E)** Mean frequency and **(F)** absolute numbers of CD4$^+$ and CD8$^+$ T cells in the spleen of non-infected (ctr) and infected mice. **(G)** Mean frequency and **(H)** absolute numbers of GzB$^+$CD4$^+$ and GzB$^+$CD8$^+$ T cells. Mice individually analyzed at day 14 pi (n=4); error bars= SEM. Data are representative of 6 independent experiments.

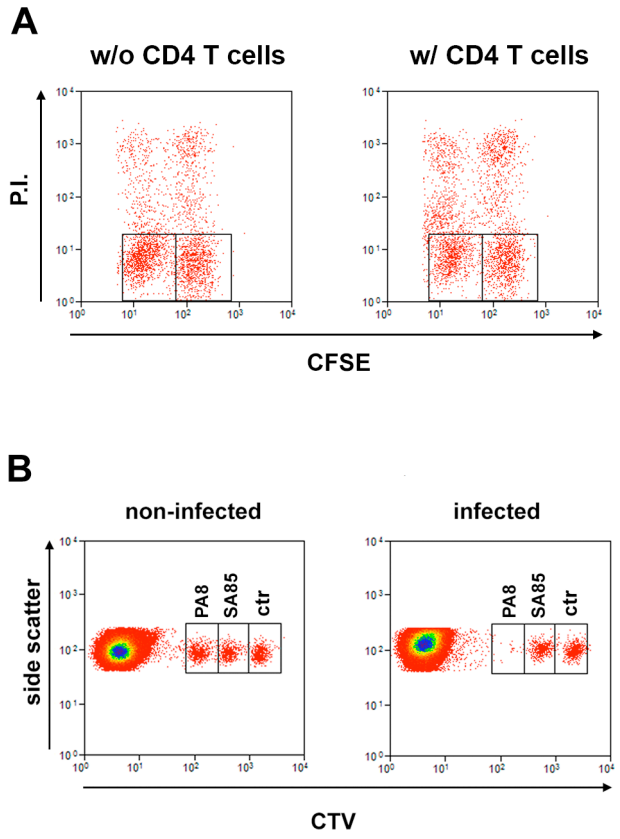

Figure 2-figure supplement 1: Gating strategy of cytotoxic assays. (A) Gating strategies and PI staining of IC-21 macrophages loaded with total amastigote protein extract ($CFSE^{lo}$) or not ($CFSE^{hi}$) and cocultured with 4 x 10^5 purified $CD4^+$ T cells (right), or not (left); specific cytotoxicity values are shown in **Figure 2B**; **(B)** Gating strategies for CTV-stained target splenocytes, loaded with the indicated antigenic peptides or not (ctr), 20 h after i.v. injection in non-infected or Y strain-infected mice. The *T. cruzi*-derived PA8 (class I-restricted) and SA85 (class II-restricted) peptides were employed. Specific cytotoxicity values for the *in vivo* assay are shown in **Figure 2C**.

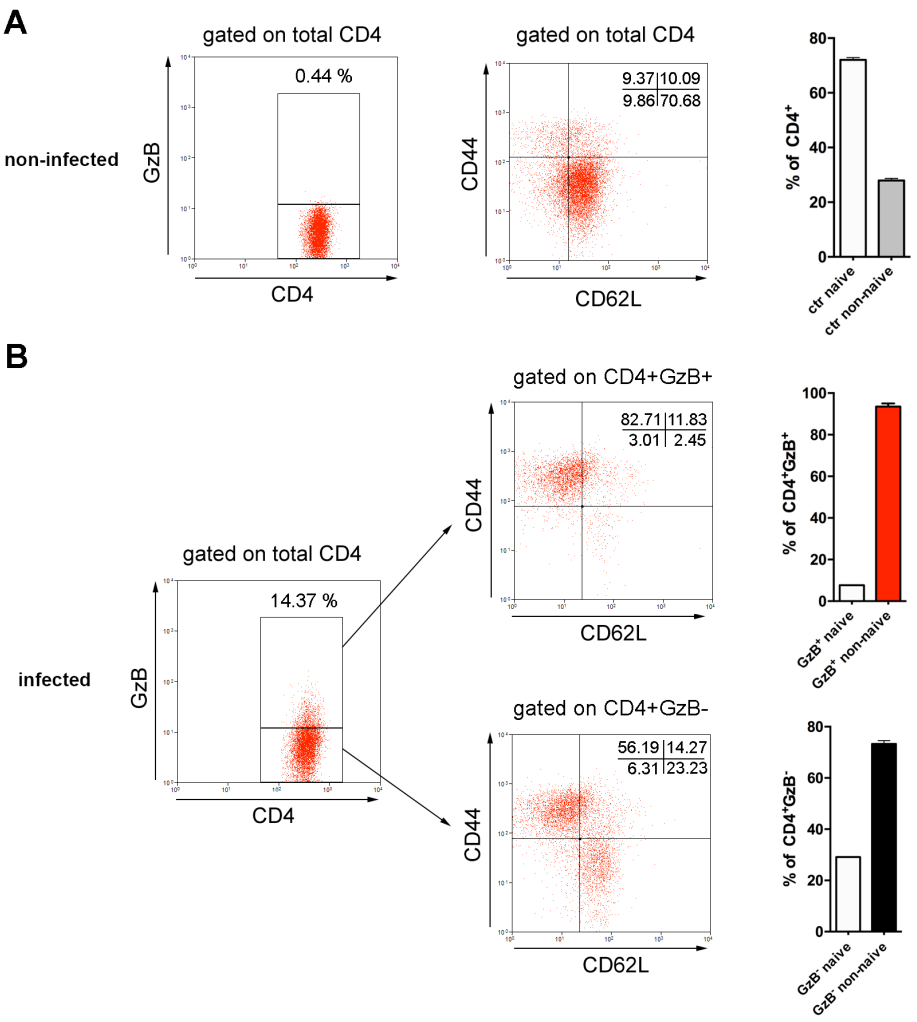

Figure 2-figure supplement 2: The majority of GzB$^+$CD4$^+$ and GzB$^-$CD4$^+$ T cells is composed of non-naive (activated effectors and memory cells). Representative dot plots and gating strategy of staining for GzB, CD44 and CD62L (on the left) and mean frequency of naive (CD44^{lo}) and non-naive (CD44^{hi}) CD4$^+$ T cells (on the right) in: **(A)** non-infected mice and gated on total CD4$^+$TCRβ$^+$ and **(B)** infected mice and gated on GzB$^+$ (top) or GzB$^-$ (bottom) CD4$^+$TCRβ$^+$ cells, at day 14 pi. Bars represent mean values of cell frequency of individually analyzed mice; n=4; Error bars = SEM. Data are representative of 3 independent experiments.

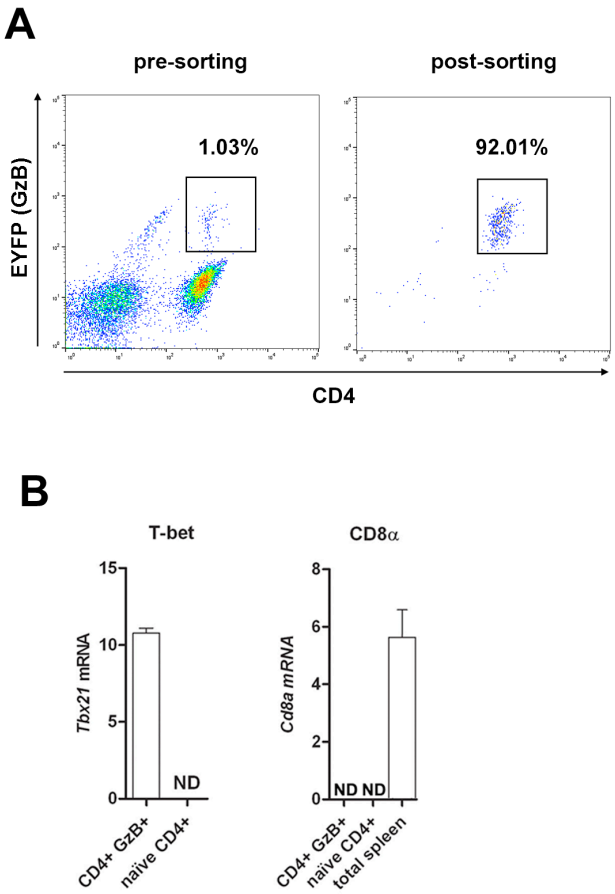

Figure 2-figure supplement 3: Expression of *Tbx21* and *Cd8a* in sorted GzB$^+$CD4$^+$ T cells. (A) Sorting gate and frequency of CD4$^+$GzB$^+$ (EYFP)$^+$ T cells obtained from infected and tamoxifen-treated GzmbCreER^{T2}/ROSA26EYFP mice. CD4$^+$ cells were enriched by negative selection with magnetic beads, as described in Methods, and then submitted to FACS-sorting. Pre-sorting CD4$^+$ T cell frequency is shown on the left panel and post-sorting on the right. **(B)** Sorted cells had RNA extracted and *Tbx21*, *Runx3d*, *Zbtb7b* and *Cd8a* expression tested by qRT-PCR, as described in Methods. Results for *Runx3d* and *Zbtb7b* expression are shown in **Fig. 2H.** ND = not detected.

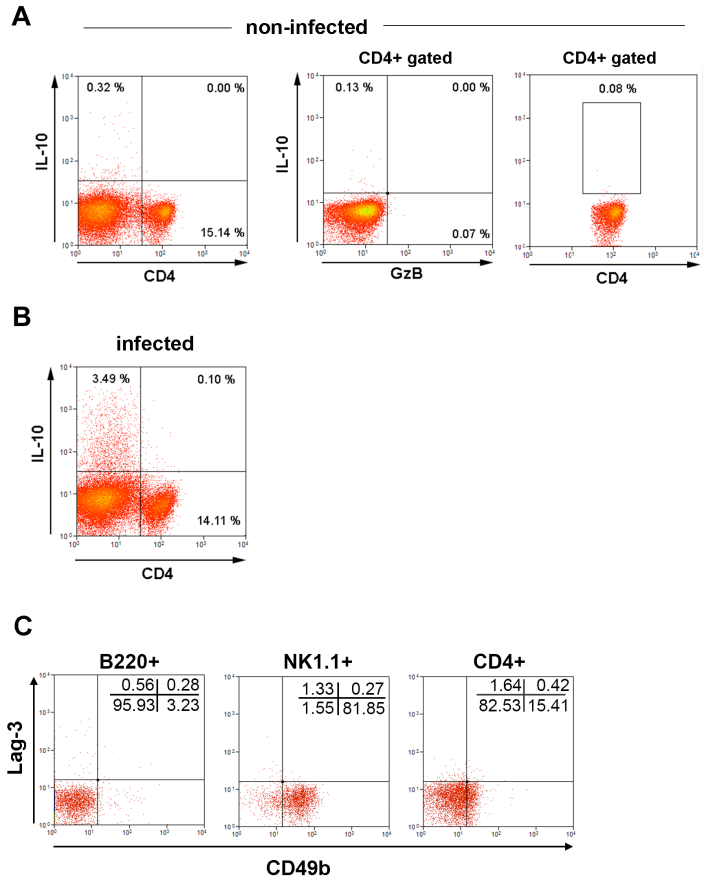

Figure 3-figure supplement 1: IL-10, Lag-3 and CD49b expression. (A) Representative dot plots and gating strategy for IL-10 expression. Total spleen cells (left) and gated $CD4^+$ T cells (middle and right panels) of non-infected control mice. **(B)** Representative dot plot of IL-10 staining in total splenocytes of infected mice. Dot plot and mean frequencies of IL-10^+ cells among $CD4^+GzB^-$ and $CD4^+GzB^+$ T cells in infected mice are shown in **Fig. 3A. (C)** Representative dot plot of Lag-3 and CD49b expression on gated $B220^+$, $NK1.1^+$ or total $CD4^+$ T cells from the spleen of non-infected mice (left, middle and right panels, respectively). Mean frequencies of Lag-3^+CD49b^+ and Lag-3^+CD49b^- cells among $CD4^+GzB^-$ and $CD4^+GzB^+$ T splenocytes of infected mice are shown in **Fig. 3C.** Data are representative of 2 independent experiments.

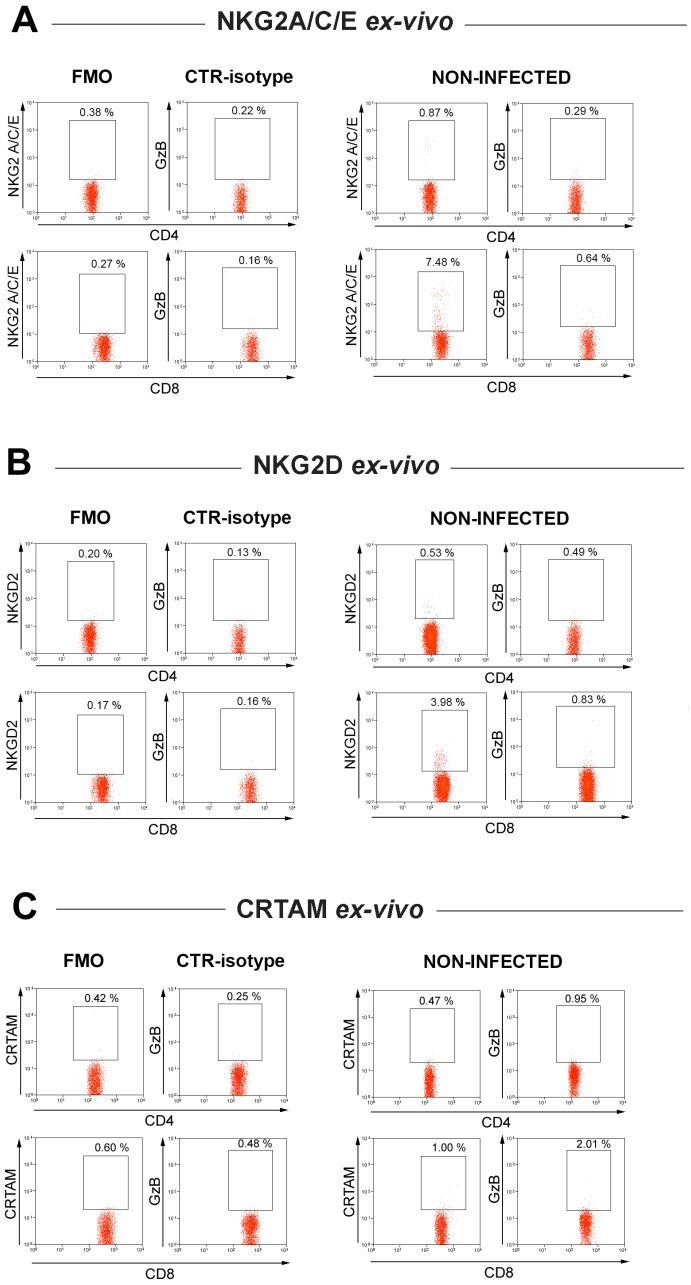

Figure 3-figure supplement 2: Representative dot plots and gating strategies for NKG2A/C/E, NKG2D and CRTAM staining on CD4$^+$ and CD8$^+$ GzB$^+$ T cells. Staining of spleen cells from non-infected controls (right panels) and FMO and isotype controls of spleen cells from B6 infected mice (left panels) are shown. Representative dot plots and mean frequencies of CD4$^+$GzB$^+$ and CD8$^+$GzB$^+$ T cells

expressing these cytotoxic markers are shown in **Figure 3F-H** and Figure 3-figure supplement 3, respectively.

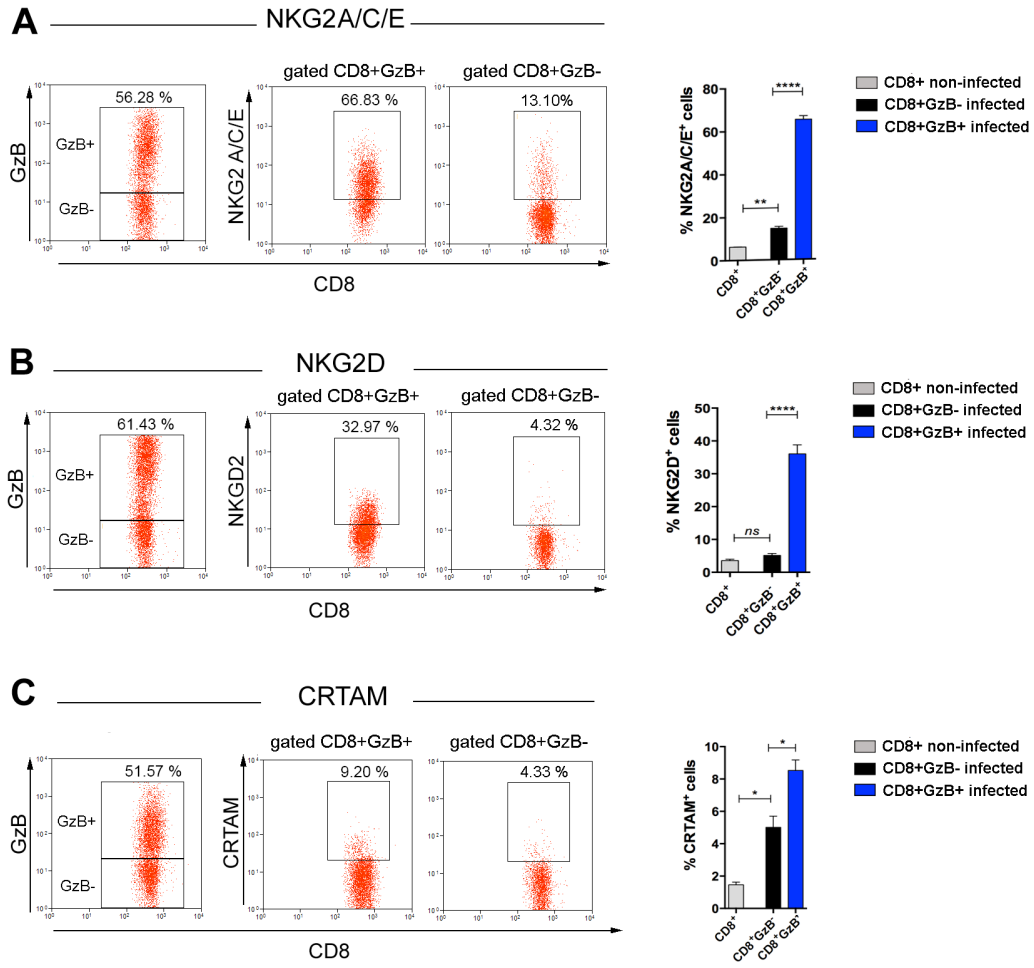

Figure 3-figure supplement 3: Expression of NKG2A/C/E, NKG2D and CRTAM cytotoxic markers by CD8$^+$GzB$^+$ T cells. Representative dot plots and gating strategies of spleen cells from B6 infected mice (left panels). Graphs on the right: bars represent mean values of cell frequency of each indicated cell subpopulation in individually analyzed mice; n=4; Error bars = SEM. Data are representative of 3 independent experiments.

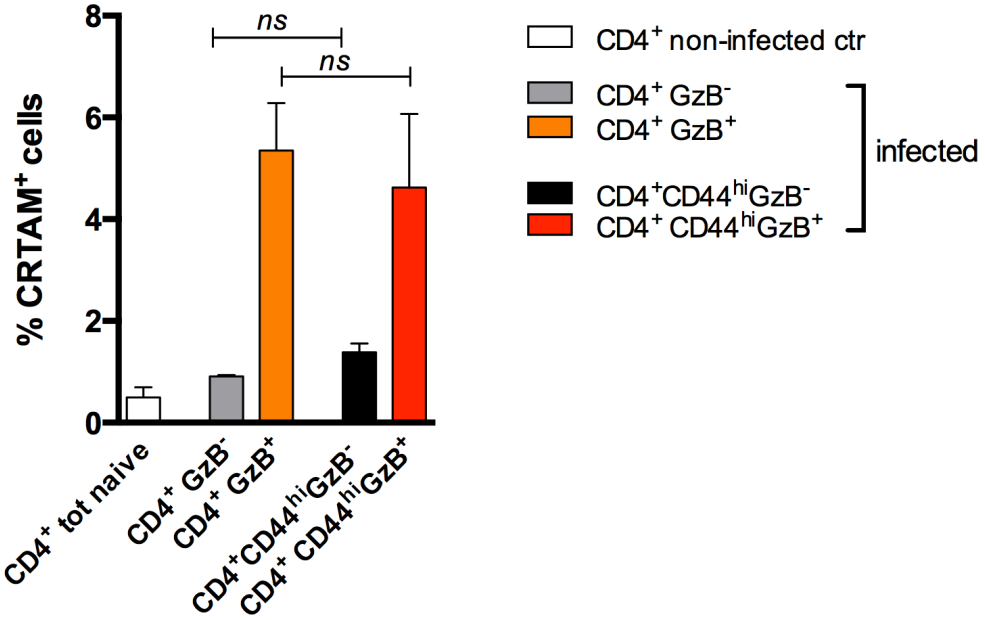

Figure 3-figure supplement 4: Frequency of CRTAM-expressing cells among splenic GzB$^+$ and GzB$^-$ CD4$^+$ T cells, gating or not on CD44^{hi} cells. Bars represent mean values of the frequency of CRTAM$^+$ cells among: CD4 naive cells of non-infected (ctr) mice (white bar) and CD4$^+$GzB$^-$ (gray bar), CD4$^+$GzB$^+$ (orange bar), CD4$^+$CD44^{hi}GzB$^-$ (black bar) or CD4$^+$CD44^{hi}GzB$^+$ (red bars) of infected mice at day 14 pi; Gating as shown in **Sup. Figs. 3 and 6C**. Mice were individually analyzed, n= 4; Error bars = SEM; *ns*= non-significant, Student t test.

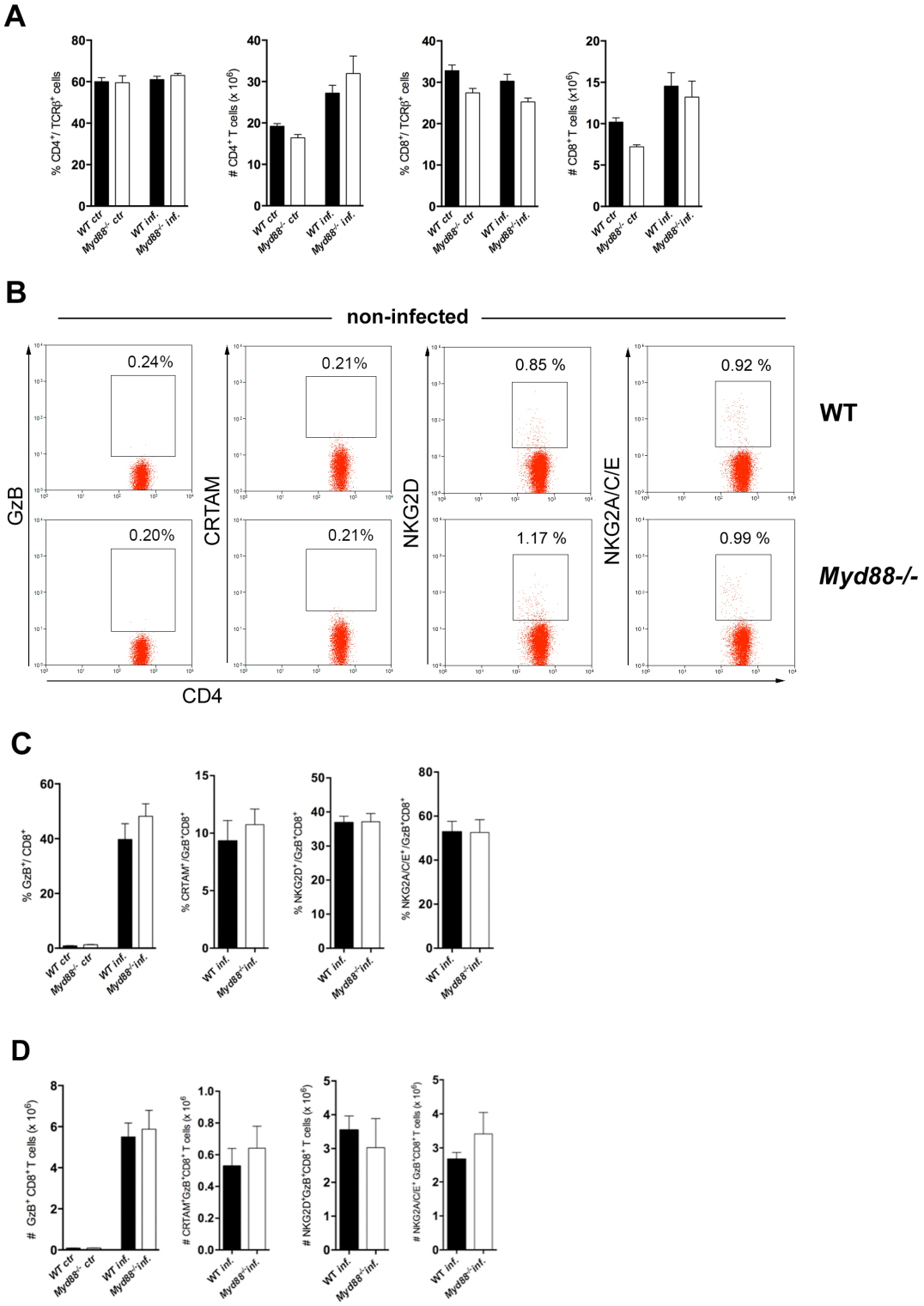

Figure 4-figure supplement 1: Equivalent frequencies and absolute numbers of total CD4$^+$ T cells in the spleens of infected *Myd88*$^{-/-}$ and WT mice. (A) Mean frequencies and absolute numbers of total CD4$^+$ and CD8$^+$ T cells in the spleens of non-infected (ctr) and infected *Myd88*$^{-/-}$ and WT (B6) mice, at day 13 pi. **(B)**

Representative dot plots and gating strategies for GzB, CRTAM, NKG2D and NKG2A/C/E staining of spleen cells from non-infected (ctr) WT (B6) and *Myd88*$^{-/-}$ mice. Staining results obtained with infected mice are shown on **Figures 4C-4E**. **(C)** Mean frequencies and **(D)** absolute numbers of GzB^{+}, GzB^{+}CRTAM^{+}, GzB^{+}NKG2D^{+} and GzB^{+}NKG2A/C/E^{+} cells among CD8^{+} T cells in the spleen of WT and *Myd88*$^{-/-}$ infected mice at day 13 pi, gated as in Sup. Fig. 7. Bars represent mean values in each group; error bars = SEM; n= 5 individually analyzed mice. Results are representative of 2 independent experiments.

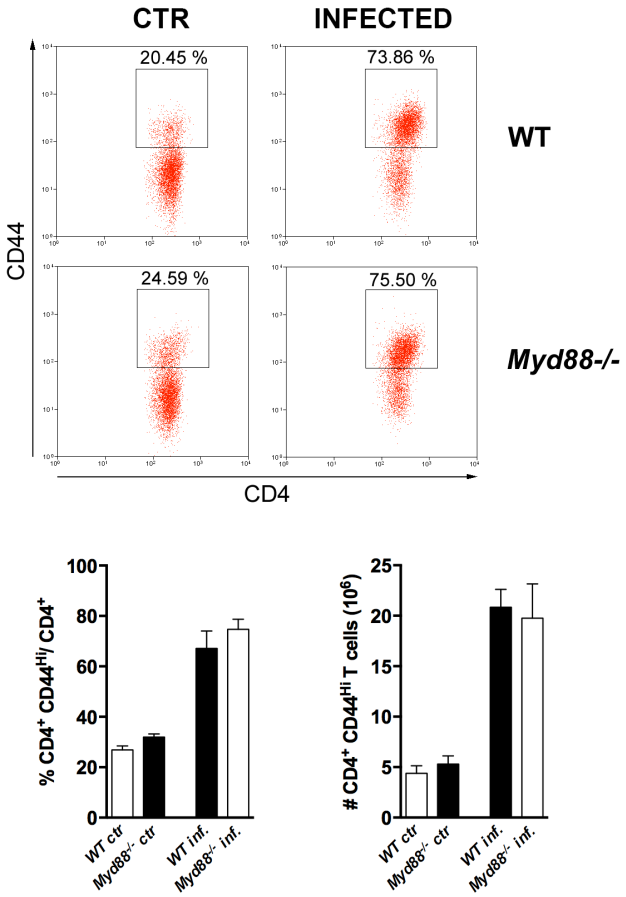

Figure 4-figure supplement 2: Equivalent frequency and absolute number of activated CD4^{+} T cells in WT and *Myd88*$^{-/-}$ mice infected with *T. cruzi.* Representative dot plots (top) and mean frequencies and absolute numbers (bottom) of CD4^{+}CD44^{hi} T cells in the spleens of infected WT (B6) and *Myd88*$^{-/-}$ mice, at day 14 pi. Mice were individually analyzed; n=4; error bars = SEM. Representative of 2 independent experiments.

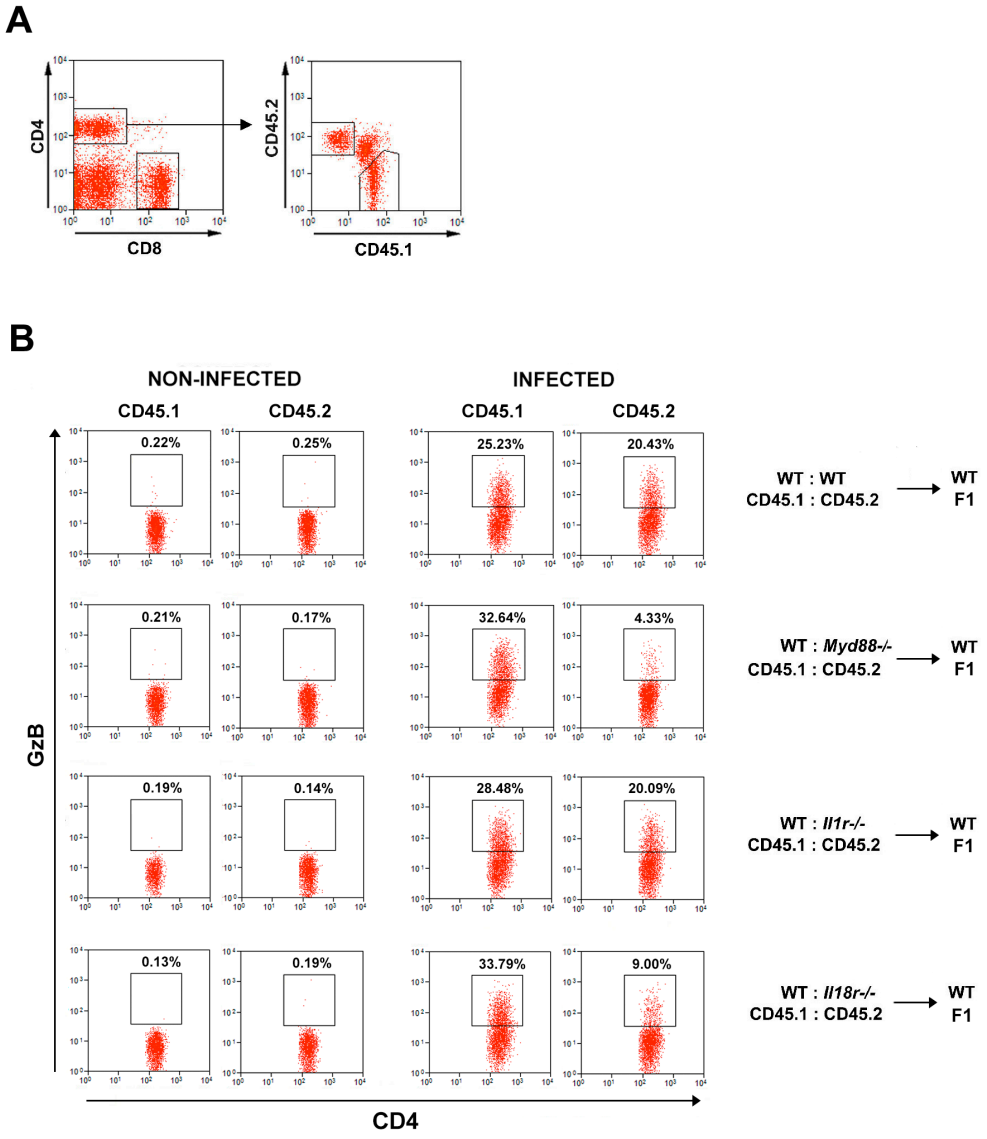

Figure 5-figure supplement 1: GzB expression in CD4$^+$ T cells of mixed-BM chimeric mice. Gating strategy and representative dot plots of: **(A)** CD45.1$^+$ and CD45.2$^+$ cells (on the right) gated CD4$^+$CD8$^-$ T lymphocytes (on the left) from the spleens of mixed-BM chimeric mice. **(B)** GzB expression in CD4$^+$CD45.1$^+$ (WT) and CD4$^+$CD45.2$^+$ (WT or KO) T cells from the spleens of non-infected and infected chimeric mice at day 14 pi, gated as in **(A).** Mean frequencies and absolute numbers of CD4$^+$GzB$^+$ in each group are shown in **Figure 5F**.

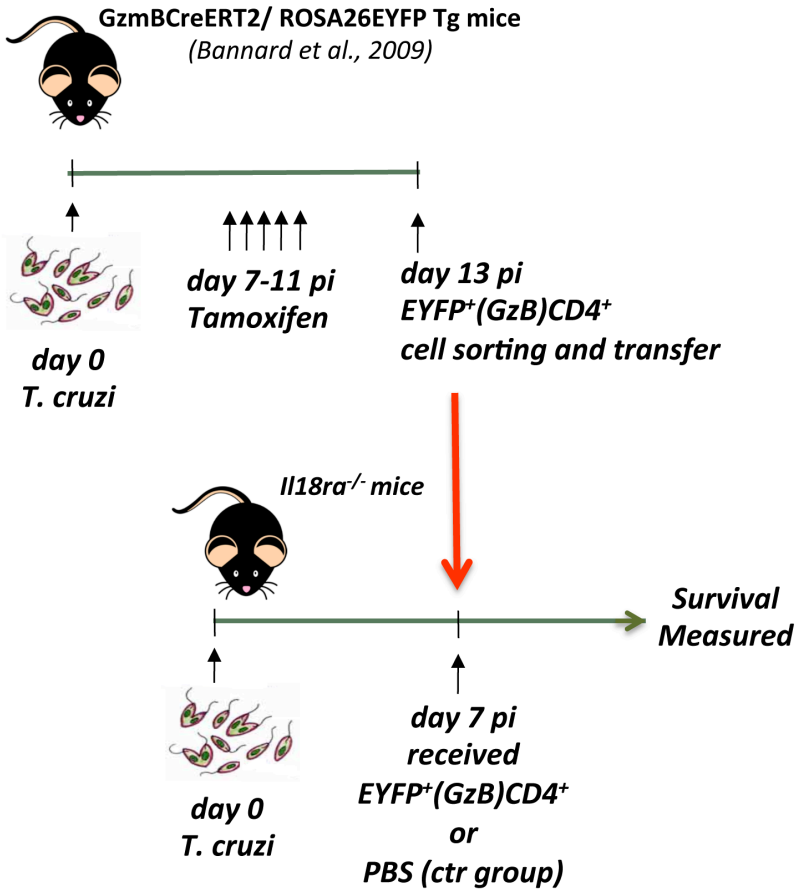

Figure 6-figure supplement 1: Time-line of the adoptive transfer experiment shown on Figure 6G.

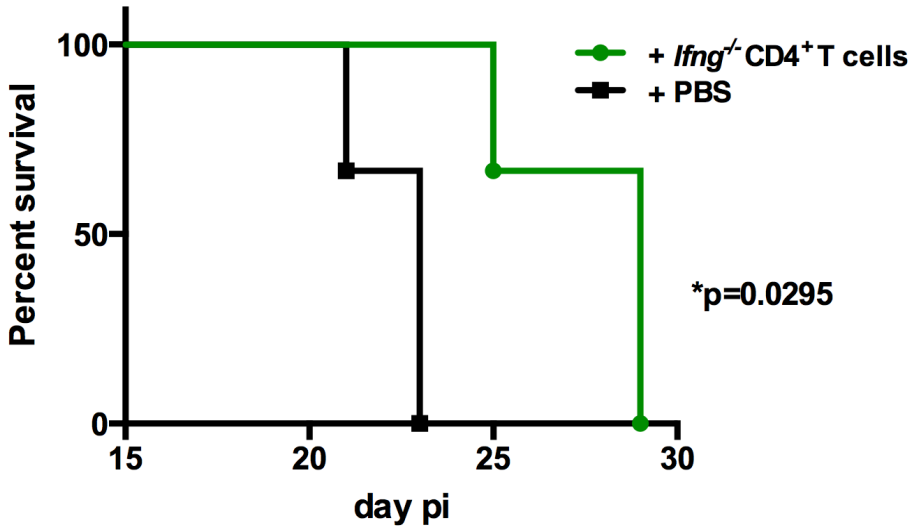

Figure 6-figure supplement 2: The adoptive transfer of *Ifng*$^{-/-}$ CD4^{+} T cells increased survival to infection. Survival curve of *Il18ra*$^{-/-}$ mice, infected with 1 x 10^3 trypomastigotes of the Y strain and adoptively transferred with sorted (>98% pure) *Ifng*$^{-/-}$ CD4^{+} T cells (green curve), or not (PBS group, black curve); n=6 mice in each group; p= 0.0295 Log-rank (Mantel-Cox) test.

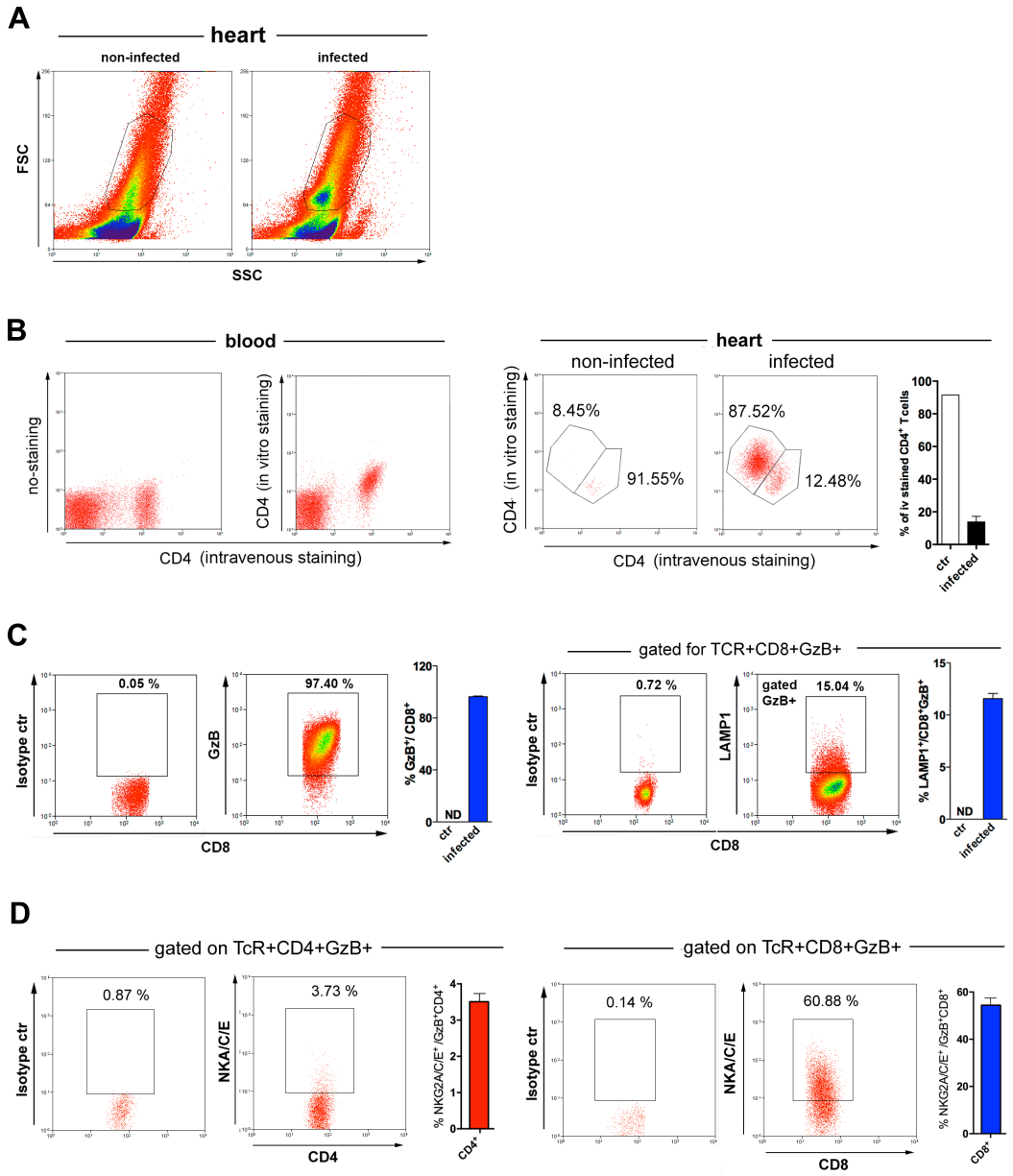

Figure 7-figure supplement 1: CD4$^+$ and CD8$^+$ T cells in the heart of mice infected with *T. cruzi*. (A) Representative FSC x SSC dot plots and gating strategy of cells from the hearts of non-infected (left panel) and infected (right panel) WT mice, employed for data analysis shown on this figure and Figure 7. **(B)** Representative dot plots of blood samples from infected mice injected iv with anti-CD4-FITC mAb, 3 min before euthanasia: with no other staining (left panel) or after staining with anti-

CD4-PECy7 mAb *in vitro* (right panel). Representative dot plots of cells from the heart of non-infected and infected mice, injected *iv* with anti-CD4-FITC mAb and stained *in vitro* with anti-CD4-PECy7 (two panels on the right), and mean frequencies of intravenously stained $CD4^+$ T cells in the hearts of non-infected and infected mice. Mice were individually analyzed; n=3; error bars = SEM. Representative of 2 independent experiments. **(C)** Representative dot plots and gating strategy of isotype and GzB (left panels) or LAMP1 (right panels) staining and corresponding mean frequencies of GzB^+CD8^+ and $LAMP1^+CD8^+$ cells among gated $CD8^+$ T cells infiltrating the infected myocardium at day 14 pi. **(D)** Representative dot plots of isotype and NKG2A/C/E staining on gated $CD4^+GzB^+$ (left panels) or GzB^+CD8^+ (right panels) T cells and corresponding mean frequencies of $NKG2A/C/E^+$ cells among GzB^+CD4^+ and GzB^+CD8^+ T cells infiltrating the infected myocardium at day 14 pi. Individually analyzed mice, n= 4; error bars= SEM; ND= not detected. Data are representative of 2 independent experiments.

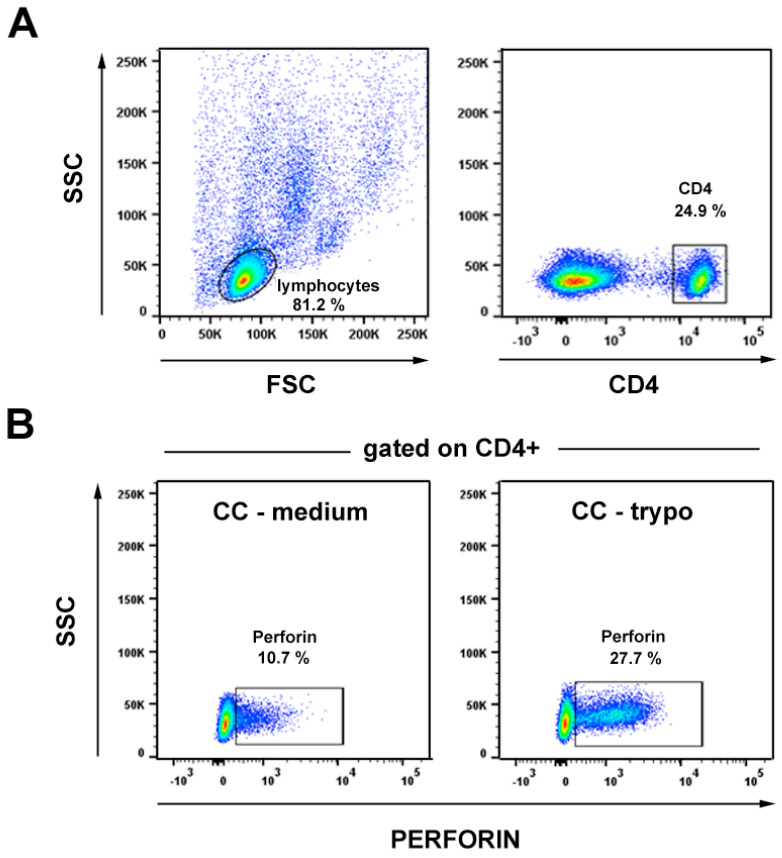

Figure 7-figure supplement 2: CD4$^+$ T cells expressing PRF are found in the circulation of patients suffering from chronic Chagas cardiomyopathy (CC). (A) Dot plot showing the gating strategy for CD4$^+$ T cell staining on PBMC. **(B)** Gating strategy and representative dot plots of PRF staining in gated CD4$^+$ T cells from CC patient incubated with medium (on the left), or with trypomastigote antigens (trypo) (on the right). Frequencies of PRF$^+$CD4$^+$ T cells and MFI of PRF staining for CC patients and HD controls are shown on **Figures 7G-7I**.

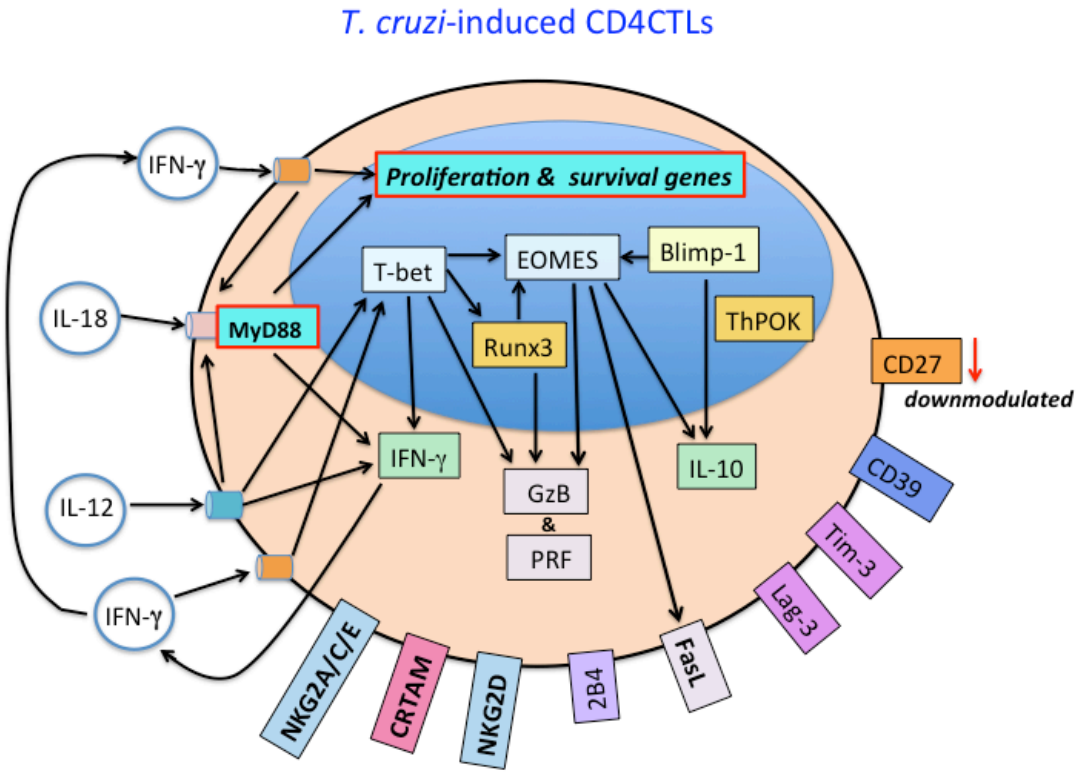

Figure 7-figure supplement 3: Predicted model for the generation of CD4CTLs cells in response to *T. cruzi* infection. This cartoon summarizes our results and also contains information of previous published studies, cited in this work. IL-12 produced during infection acts on TCR-triggered $CD4^+$ T cells, leading to T-bet expression, which promotes IFN-γ upregulation and induces *Runx3d* and *Eomes* gene expression. In turn, IFN-γ- and IL-12-signaling induce IL-18R expression. T-bet, Eomes and Runx3d drive the expression of cytotoxic effector molecules, including GzB, PRF and FasL. IL-10 expression can be induced by Blimp-1 and Eomes, although few IL-10^+ $CD4^+GzB^+$ T cells were found in our infection model. As opposed to intraepithelial CD4CTLs of the gut, ThPOK expression is not downmodulated in splenic $CD4^+GzB^+$ T cells, until day 14 pi. IFN-γ is produced by around 18% of these cells at the peak of the $CD4^+$ T cell response (14 dpi), and is necessary for $CD4^+GzB^+$ T cell proliferation and/or survival. Most $CD4^+GzB^+$ T cells express Lag-3, Tim-3 and CD39 immunoregulatory molecules, while CD27 is downmodulated. Notably, the expansion and/or survival of $CD4^+GzB^+$ T cells expressing CRTAM, NKG2D, and NKG2A/C/E cytotoxic markers depend on T-cell intrinsic IL-18R/MyD88 signaling.